Buckling analysis for EUDP offshore wind suction bucket on an industrial scale

Madsen, Søren; Gérard, Lucile

Publication date:
2016

Document Version
Publisher's PDF, also known as Version of record

Title

Buckling analysis for EUDP offshore wind suction bucket on an industrial scale

Søren Madsen
Lucile Gérard

ISSN 1901-7278
DCE Technical Report No. 213

Aalborg University
Department of Civil Engineering
Group Name

DCE Technical Report No. 213

Buckling analysis for EUDP offshore wind suction bucket on a industrial scale

by

Søren Madsen
Lucile Gérard

August 2016

Scientific Publications at the Department of Civil Engineering

Technical Reports are published for timely dissemination of research results and scientific work carried out at the Department of Civil Engineering (DCE) at Aalborg University. This medium allows publication of more detailed explanations and results than typically allowed in scientific journals.

Technical Memoranda are produced to enable the preliminary dissemination of scientific work by the personnel of the DCE where such release is deemed to be appropriate. Documents of this kind may be incomplete or temporary versions of papers—or part of continuing work. This should be kept in mind when references are given to publications of this kind.

Contract Reports are produced to report scientific work carried out under contract. Publications of this kind contain confidential matter and are reserved for the sponsors and the DCE. Therefore, Contract Reports are generally not available for public circulation.

Lecture Notes contain material produced by the lecturers at the DCE for educational purposes. This may be scientific notes, lecture books, example problems or manuals for laboratory work, or computer programs developed at the DCE.

Theses are monograms or collections of papers published to report the scientific work carried out at the DCE to obtain a degree as either PhD or Doctor of Technology. The thesis is publicly available after the defence of the degree.

Latest News is published to enable rapid communication of information about scientific work carried out at the DCE. This includes the status of research projects, developments in the laboratories, information about collaborative work and recent research results.

Published 2016 by
Aalborg University
Department of Civil Engineering
Sofiendalsvej 9-11
DK-9200 Aalborg SV, Denmark

Printed in Aalborg at Aalborg University

ISSN 1901-7278
DCE Technical Report No. 213

Recent publications in the DCE Technical Report Series

1. Initial conditions

In order to compare the suction bucket foundation behaviour with a circular cylinder, two circular cylinder geometries were considered. The first one corresponding to the monopod foundation dimensions has a radius r=9000mm, a length l=10000mm and a thickness t=17mm. t 17mmThe circular cylinder corresponding to the jacket foundation support dimensions has the following characteristics: r=5000mm, l=8000mm and t=17mm.

1.1. Boundary conditions

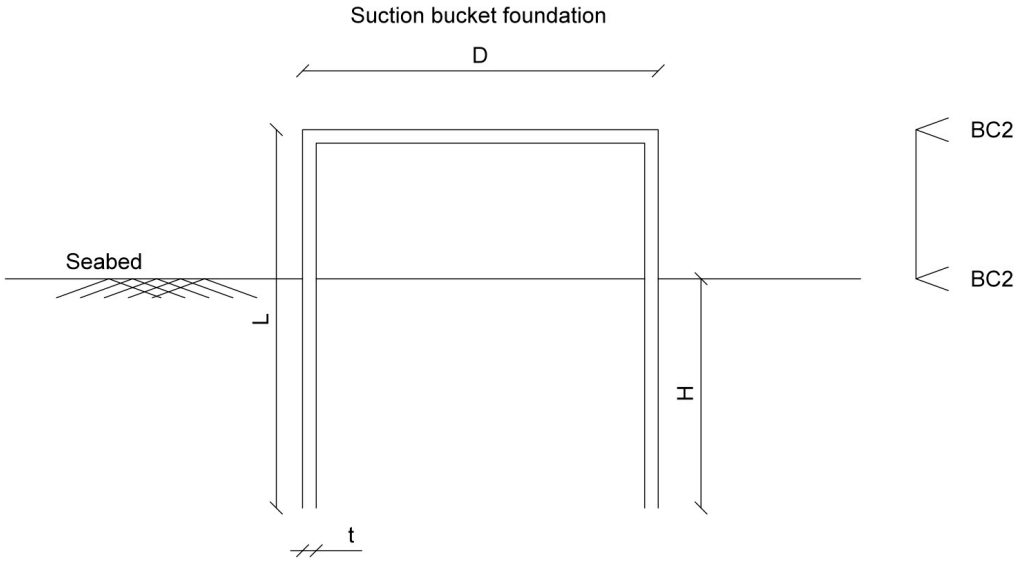

Figure 1 : Suction bucket foundation parameters and boundary conditions

The lid from the 3D STEP file has been removed and the boundary condition **BC2** corresponding to a pin connection and to the **S3** "classical" boundary condition is applied at both cylinder ends (*Figure 1*) (Madsen, Ibsen, & Andersen, 2013).

1.2. Loading

The following loading (*Figure 2)* was used to consider the hydrostatic pressure applied on the suction bucket foundation.

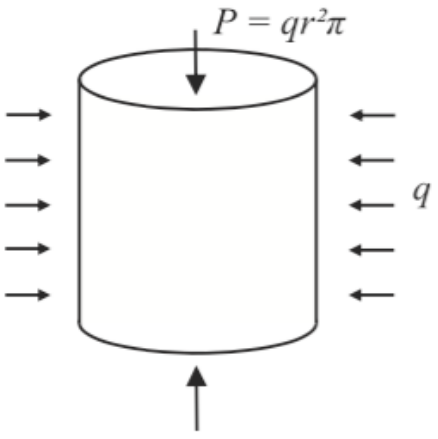

Figure 2 : Cylinder under hydrostatic pressure. (Teng & Rotter, 2004)

The load applied should be in the same order of magnitude as the critical buckling load of the structure. The *Eurocode* provides theory to calculate the critical buckling pressure under combined

loading only for a circular cylinder. Thus, q_{cr} of a circular cylinder with dimensions for each function (monopod or jacket foundation) was determined.

$$q_{cr,monopod\ foundation} = 35{,}0\ kPa = 0{,}035\ MPa$$

$$q_{cr,jacket\ foundation} = 11{,}2\ kPa = 0{,}011\ MPa$$

Hence, the following loads were applied to each structure:

- Circumferential compression: q=0,01 MPa$q = 0{,}01\ MPa$
- Axial compression (shell edge load):

$$p = \frac{P}{2\pi r} = \frac{qr}{2} = \begin{cases} 45\ N/mm\ for\ the\ monopod\ foundations \\ 25\ N/mm\ for\ the\ jacket\ foundation\ supports \end{cases}$$

1.3. Material properties

The material properties employed in the *Eurocode* were chosen for this study.
The steel used is considered elastic and perfectly plastic with a yield limit fy=355MPa$f_y = 355\ MPa$ (*Figure 3*).

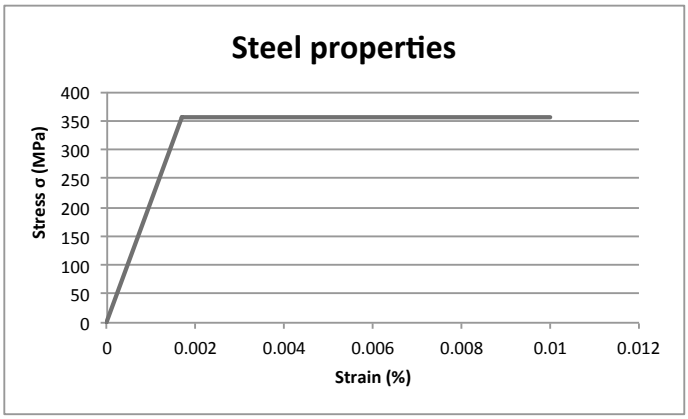

Figure 3 : Material properties

2. First round

Ib Andressen industries (IAI) designed various suction bucket foundation shapes presented in *Appendix A*. Models 1060 and 1053, bucket foundation shapes having a reference diameter D=18m and a length L=10m, are designed to be used for monopod foundation unlike models 50 to 62 which have a reference diameter D=10m and a length L=8m will be used to support jacket foundations.

A 17mm thickness was used in a first time. Then, if a bucket foundation shape resistant to buckling and using this thickness cannot be found, other solutions will be investigated.

First of all, a linear bifurcation analysis has been done for each shape in order to find an initial estimate on which shape was the more resistant to buckling. Then, the penetration depth influence on the critical buckling pressure has been studied. Finally, an imperfection influence study has been performed using a GMNIA (Geometrical and material nonlinear analysis of the imperfect structure) analysis.

2.1. Linear bifurcation analysis

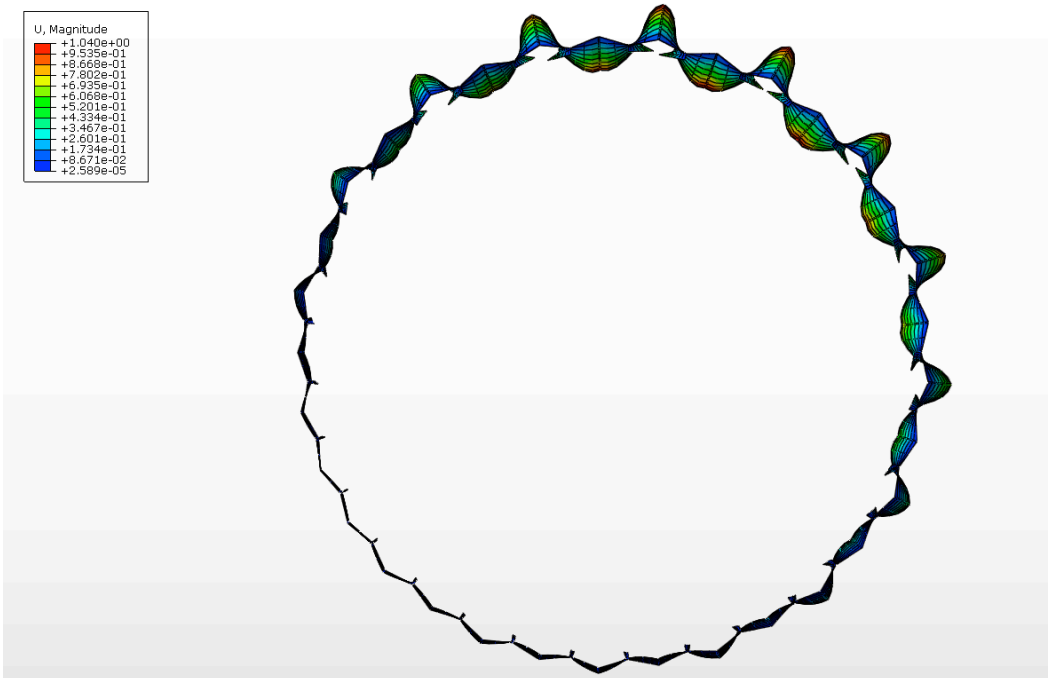

Figure 4 : First mode buckling shape, model 1053 (Z-X plane).

The buckling modes obtained and shown in *Appendix B* are unsymmetrical (*Figure 4*). This phenomenon can be explained by an interaction between the symmetrical buckling mode of a circular cylinder and the presence of the stiffeners.
Stiffeners increase the structure's buckling resistance. When the structure is stiffer, the critical buckling pressure is increased and local instability can occur before reaching the overall failure. Such instabilities can be seen in models 1053 and 53's buckling modes (*Figure 5*). The rest of the figures are shown in *Appendix C*.

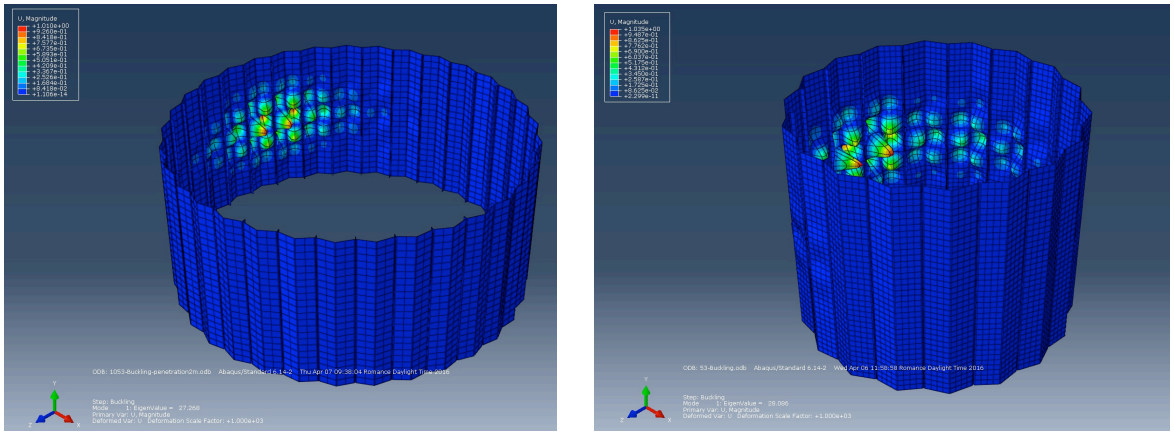

Figure 5 : First mode buckling shape, model 1053 on the left and model 53 on the right (3D).

Table 1 : Critical buckling pressure obtained for the different models.

Model	q_{cr} (kPa)	Length (m)
1053	177,1	10
1060	82,8	
50	145,9	8
51	127,0	
52	89,5	
53	280,9	
60	79,0	
62	125,7	

These analyses (*Table 1)* reveal that model 1053 and 53 give the highest critical buckling pressure.

2.2. Penetration depth influence study

In order to study the influence of the penetration depth on the critical buckling pressure, various penetration depths have been considered: 0m, 2m, 4m, 6m and 8m for models 1053 and 1060; 0m, 2m, 4m and 6m for models 50 to 62. For each length and each shape, a linear bifurcation analysis has been performed.

The numerical results shown in *Figure 6 and Figure 7* have been compared to various theories: theory from R.Greiner for medium-long cylinders under uniform external pressure (Greiner, 2004) and analytical formulas developed by *Von Mises* (Members of Structural Stability Research Council task groups and other specialits, 1998).

According to R.Greiner theory (Greiner, 2004), the critical buckling stress is calculated with the following equation:

$$\sigma_{cr} = 0{,}92E\frac{r}{l}\left(\frac{t}{r}\right)^{1{,}5}$$

The critical buckling pressure is then determined by:

$$q_{cr} = \sigma_{cr}\frac{t}{r}$$

q_{cr} $\sigma_{cr}\frac{t}{r}$

The following equation developed by *Von Mises* (1931, 1933) gives the theoretical critical buckling pressure of the perfect shell under hydrostatic pressure:

$$p_c = \frac{2E(\frac{t}{D})}{n^2 + \left(\frac{\lambda^2}{2}\right) - 1}\left\{\frac{(\frac{t}{D})^2}{3(1-\nu^2)}[(n^2+\lambda^2)^2 - 2n^2 + 1] + \frac{\lambda^4}{(n^2+\lambda^2)^2}\right\}$$

Where:

$$n: number\ of\ circumferential\ lobes$$

$$\lambda = \frac{\pi D}{2L}$$

The number of circumferential lobes n to use is the one giving the lower value of p_c.

Note that these theories consider a circular cylinder without stiffeners.

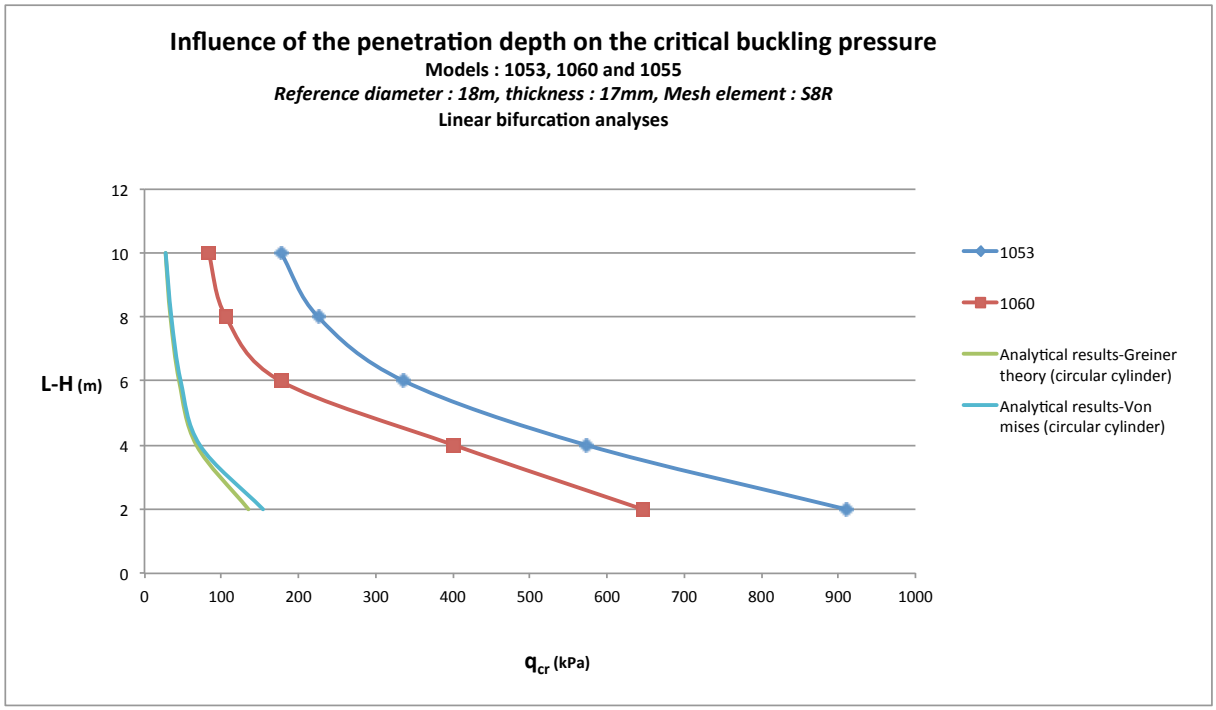

Figure 6 : Penetration depth in function of the critical buckling pressure, models 1053 and 1060.

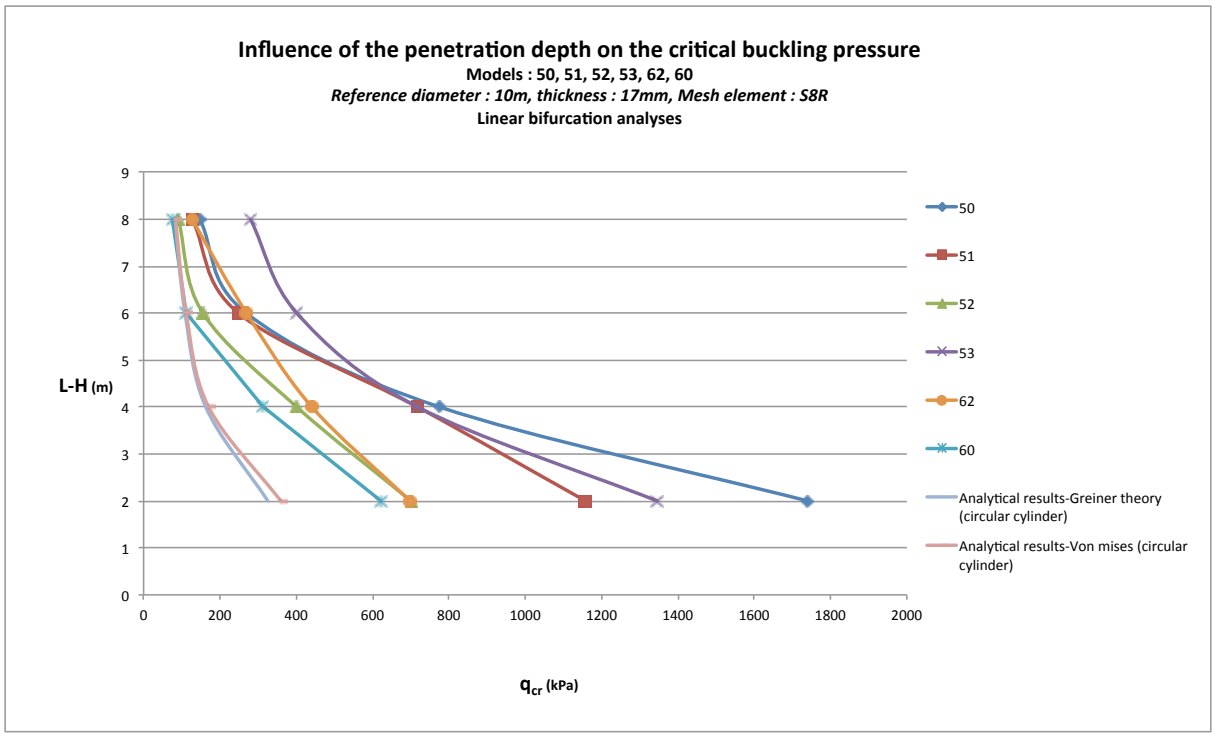

Figure 7 : Penetration depth as a function of the critical buckling pressure, models 50,51, 52, 53, 60 and 62.

All of the enhanced shapes behave stronger against buckling than a circular cylinder as shown with the analytical curves in *Figure 6* and *Figure 7*.

Models 1053 and 53 seem to be the more reliable models: local instability occurs due to high stiffness and the critical buckling pressure is higher than for the other models. This phenomenon can be seen in the buckling shape presented in *Annex C*, *Figure 40* and *Figure 45*.

2.3. Imperfection's influence on the critical buckling pressure

First of all, imperfection sensitivity analyses were performed on model 1053.
The parameter α corresponds to the imperfection input in Abaqus.

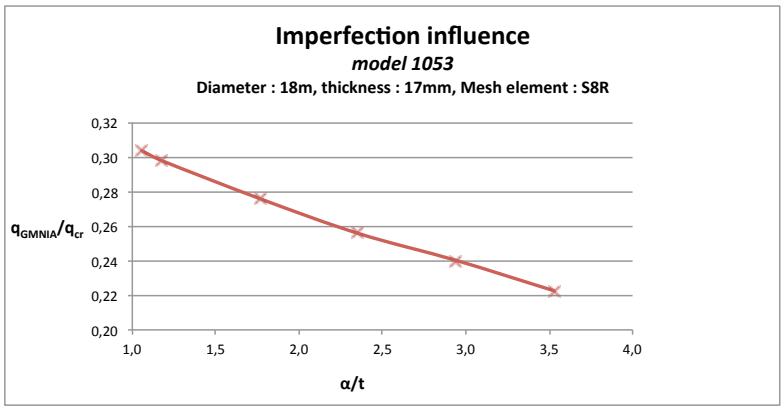

Figure 8 : knockdown factor as a function of the ratio α/t.

Knockdown factors obtained in *Figure 8* are low and seem to keep dropping as the imperfection size increases. The monopod bucket foundation shape 1053 is highly imperfection sensitive. Further in the project, GMNIA analyses considering more imperfection sizes have been performed in order to have a better prediction of the final knockdown factor.

3. Second round

In order to find the most buckling resistant bucket foundation shape, enhanced drawings were made and imperfection analyses were performed for each shape available at this step.

3.1. Penetration depth influence study, linear bifurcation analyses

The first results showed that the buckling resistance increases with the segment number and presence of bends. To verify this phenomenon, model 1055 corresponding to model 1053 "cookie cutter" with more segments and more bends was drawn and tested.

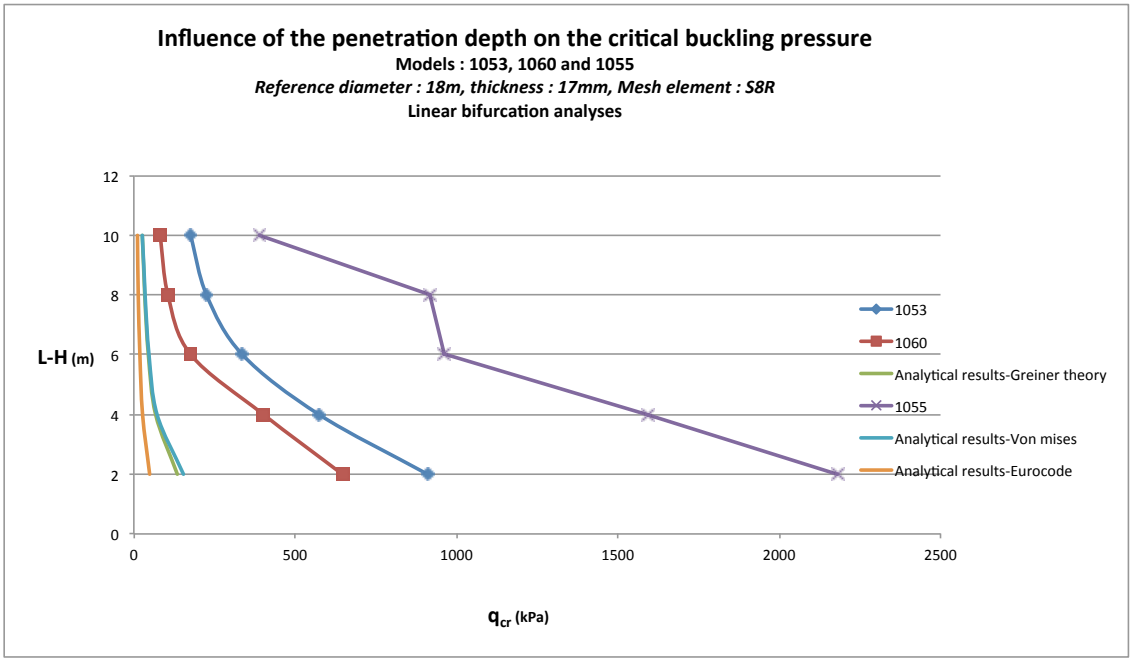

Figure 9 : Penetration depth as a function of the critical buckling pressure, models 1053, 1060 and 1055.

Results in Figure 9 show that the monopod bucket foundation with shape 1055 is stronger against buckling than the other enhanced shapes.

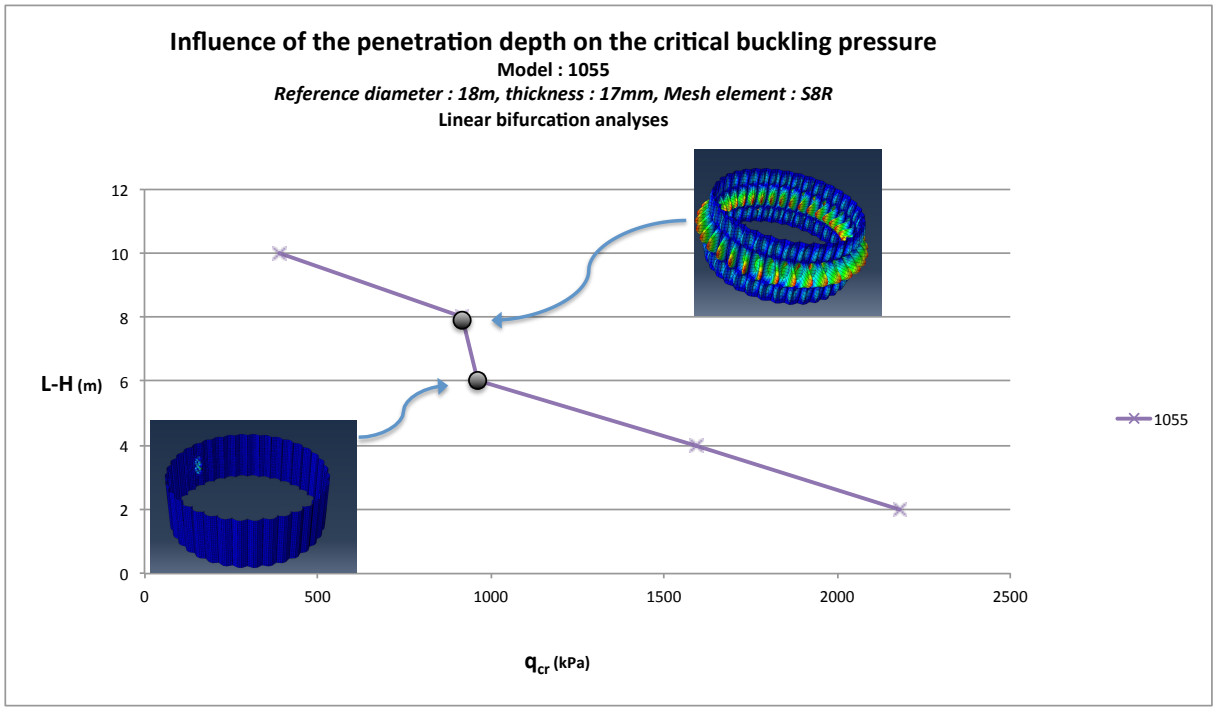

Figure 10 : Penetration depth as a function of the critical buckling pressure and buckling shapes for a penetration depth of 2m and 4m, model 1055.

The similarity between the results of the linear bifurcation analysis performed for the enhanced shape 1055, in the case of a penetration depth of 2m and 4m (L-H=8m and L-H=6m) can be explained by the difference of failure modes (*Figure 10*).
Indeed, for a 4m penetration depth (L-H=6m), the overall failure is due to local buckling and is happening before overall buckling because of the higher stiffness of the structure. It can be assumed that the overall failure of the structure will occur at a higher load.

3.2. Imperfection sensitivity

It has been shown above that a structure can seem highly resistant to buckling on the linear analysis whereas its imperfection sensitivity will induce an important drop of its strength.
To this end, GMNIA analyses were performed for each model with various imperfection sizes. For each analysis, the first buckling mode shape was introduced although the various enhanced bucket foundation shapes did not provide the same buckling shapes: some of them were symmetric whereas others were unsymmetrical. Further in the project, the worst buckling shape will be sought for each bucket foundation pattern.

A comparison with the semi-empirical knowledge from the *Eurocode* (Eurocode EN 1993-1-6) has also been made.

The figures shown in *Appendix D* present the results of the nonlinear analyses for each enhanced shape. For several ratios α/t, the load displacement curve is showed with the critical buckling point specified.

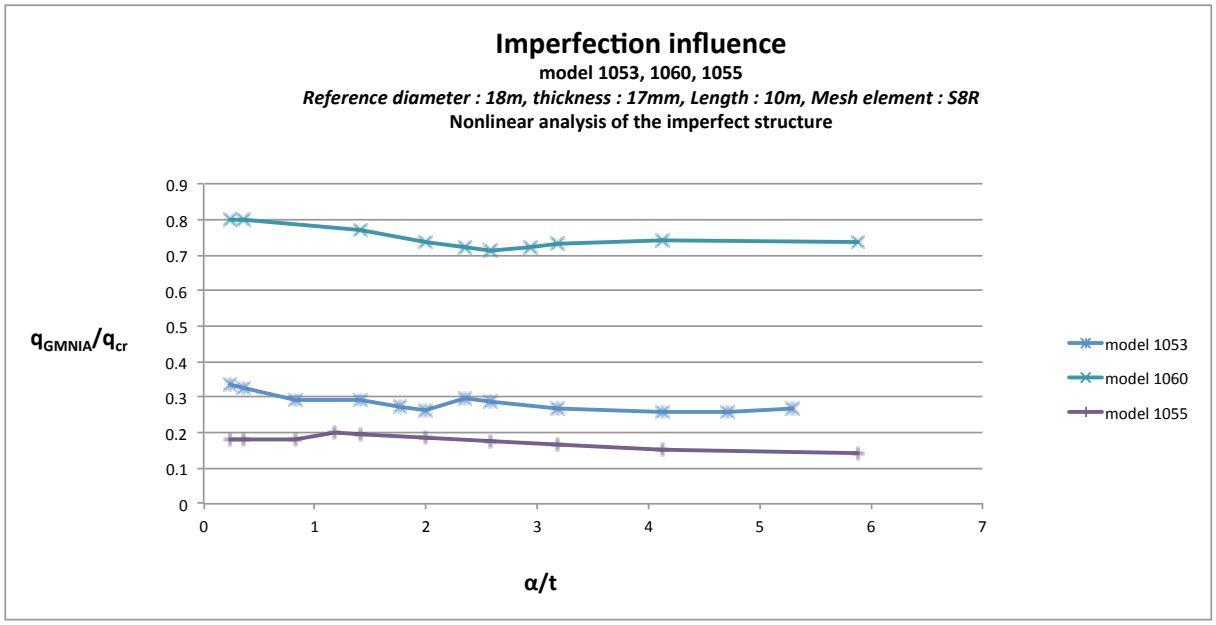

Figure 11 : knockdown factors as a function of the ratio α/t, models 1053, 1060 and 1055.

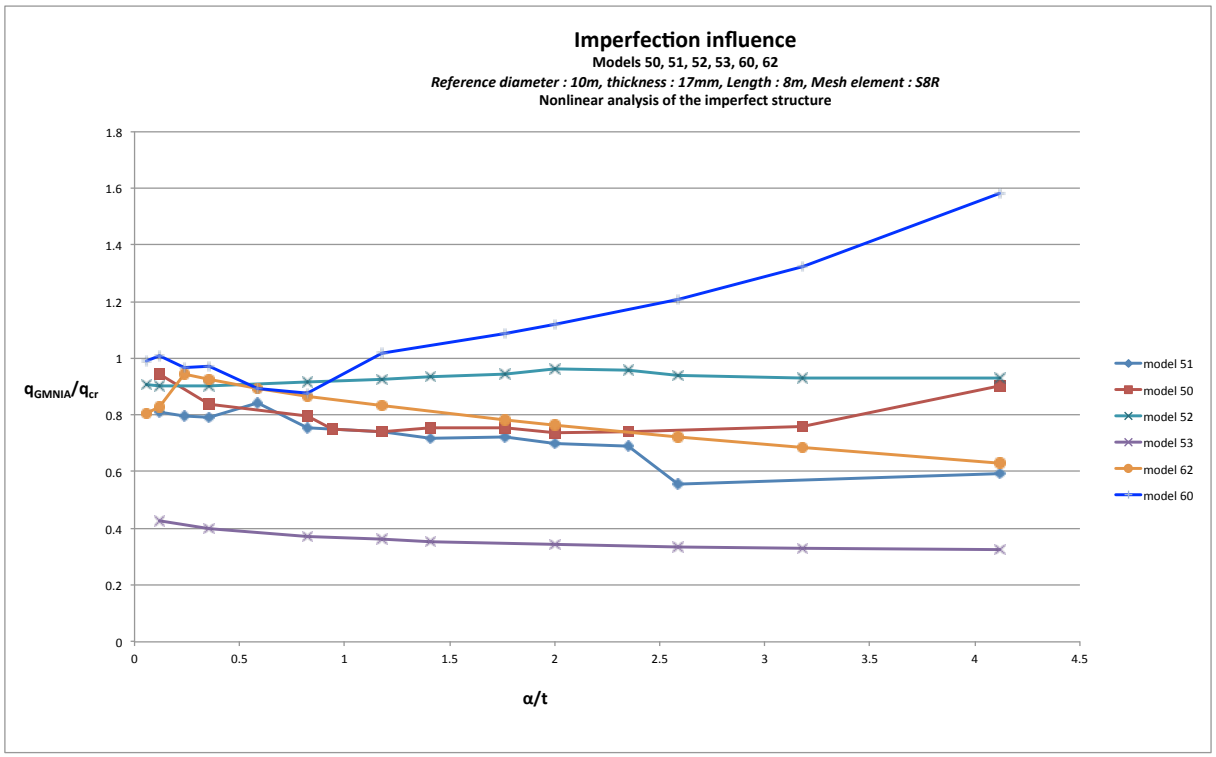

Figure 12 : knockdown factors as a function of the ratio α/t, models 50, 51, 52, 53, 60 and 62.

The results obtained and shown in *Figure 11* and Figure 12 point out various behaviours to the presence of imperfections. Two imperfection sensitivity characteristics can be seen: the sensitivity to the presence of an imperfection by inducing an important drop in the critical buckling pressure and the sensitivity to the imperfection size when the curve obtained is not constant with the variation of the imperfection size.

Regarding the monopod foundations, all of the enhanced shapes considered are not sensitive to the imperfection size although model 1055 strength reduces by almost 90% when imperfections are included no matter their size.

Respecting to the jacket foundation supports, as well as monopod foundations, models 53 and 52 do not show sensitivity to the imperfection size although model 53 is highly sensitive to the presence of imperfection.

On the other hand, models 50, 51, 60 and 62 are sensitive to the size of the imperfection. For high ratios α/t , the knockdown factor rises (model 50) thanks to the stress redistribution or becomes constant (model 51).

Stress redistribution:

When certain imperfections are included on the structure, stress redistribution can occur. That is why critical buckling loads higher than the predicted linear result are found.
GMNIA analyses are performed in order to find the appropriate imperfection to introduce to predict the real behaviour of the structure. Thus, imperfections giving these results should not be chosen.

The knockdown factors and the critical buckling pressure of the imperfect structures derived from for each model are shown in *Table 2.* The knockdown factors chosen are the ones where the curves in Figure 11 *and* Figure 12 show a threshold or a minimum.
In the case of the enhanced shape 62, none of these conditions can be seen. Hence, the last value corresponding to a realistic imperfection size with a ratio α/t=4,1 is chosen.

In order to approach as close as possible the real behaviour of the structure, experimental tests should be performed.

Table 2 : knockdown factors and critical buckling pressure of the imperfect structures.

Knockdown factors, enhanced shapes				
	Critical buckling pressure			
	model	q_{cr} (kPa) - *LBA*	knockdown factor	$q_{cr,imp}$ (kPa) - *GMNIA*
Jacket foundation *(L=8m)*	50	145,93	0,70	102,15
	51	127,02	0,55	69,86
	52	89,46	0,90	80,51
	53	280,86	0,32	89,88
	60	79,01	0,86	67,95
	62	125,70	0,62	77,93
	55	748,78	0,22	164,73
Monopod foundation *(L=10m)*	1053	177,05	0,25	44,26
	1060	82,77	0,70	57,94
	1055	388,05	0,15	58,21

3.3. Penetration depth influence study, nonlinear analyses of the imperfect structures

The critical buckling pressure values for each enhanced shape and each penetration depth have been multiplied by the knockdown factors obtained with the GMNIA analysis in order to point out the behaviour of the imperfect structure.

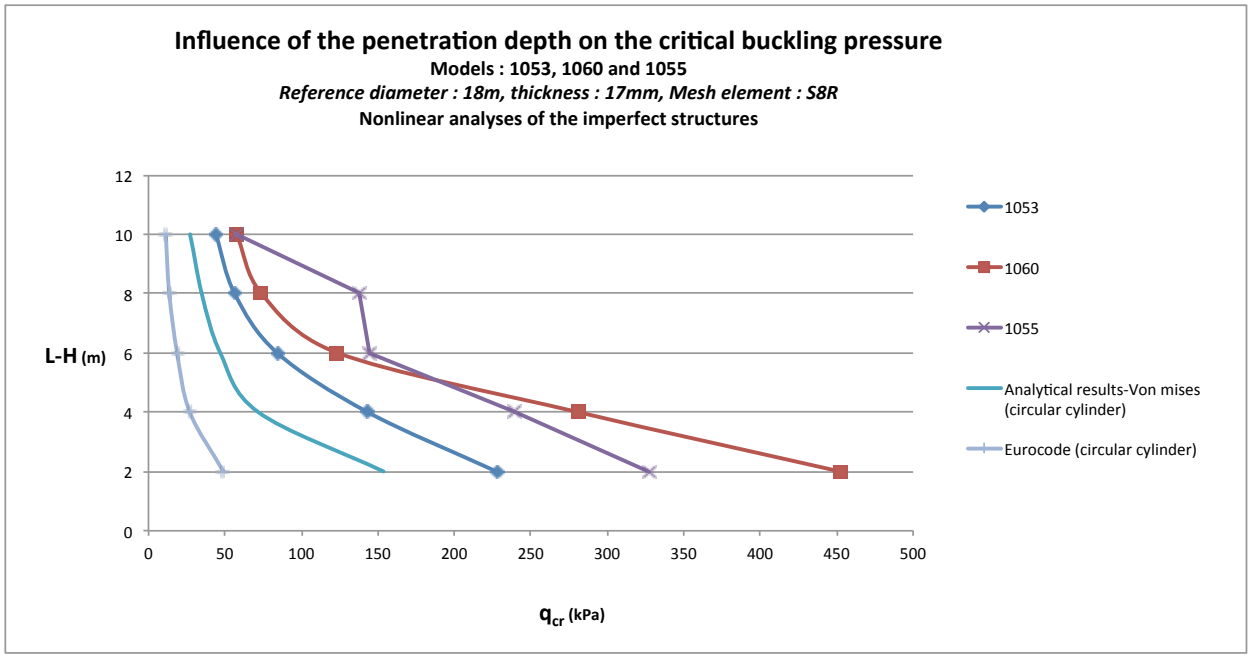

Figure 13 : Penetration depth as a function of the critical buckling pressure, models 1053, 1060 and 1055, nonlinear analyses. The KDF obtained for a bucket foundation length of 10m was applied on each length.

Among the monopod bucket foundations (*Figure 24*), model 1053 is less reliable because of its high imperfection sensitivity whereas model 1060 seems to be more resistant to buckling when the imperfect structure is considered.
Although the enhanced shape 1055 is highly imperfection sensitive, the structure is still interesting regarding its behaviour against buckling.

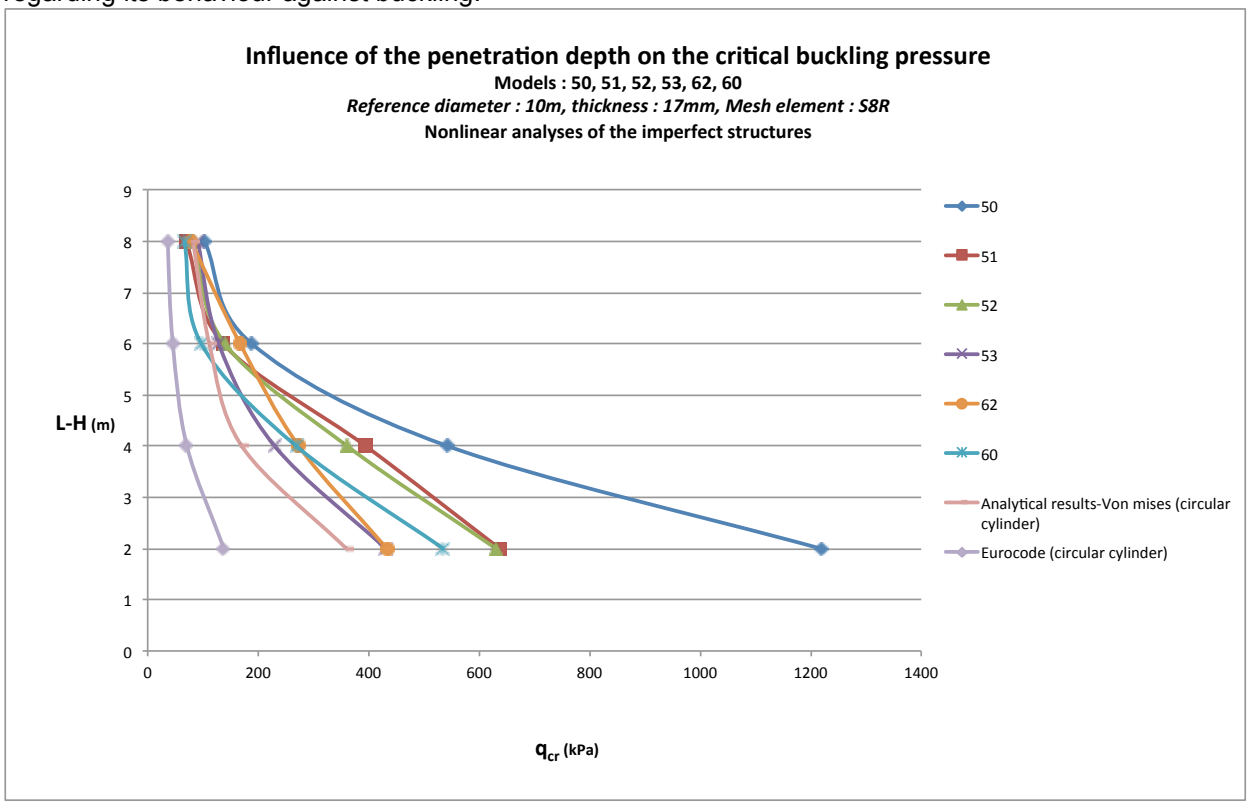

Figure 14 : Penetration depth as a function of the critical buckling pressure, models 50,51, 52, 53, 60 and 62, nonlinear analyses. The KDF obtained for a bucket foundation length of 8m was applied on each length.

On the other hand, among the jacket foundation supports (*Figure 25*), models 60 and 62 are still the less buckling resistant.

Moreover, because of its high sensitivity to the presence of imperfections, model 53 is no longer the most reliable shape studied.
The enhanced shape 50, thanks to its low imperfection sensitivity, keeps a significant critical buckling pressure.

The previous studies conducted revealed a strong behaviour of shape 1055 against buckling. Thus, the characteristics of these shapes, i.e one more bend per elements and more elements than shape 1053 were applied on the supports for jacket foundations. To that end, Andresen design team drew shape 55 satisfying these conditions.

4. Linear bifurcation analyses, shape 55

Firstly, linear bifurcation analyses were performed on shape 55 to obtain a linear prediction of the critical buckling pressure depending on the penetration depth of the suction bucket foundation.

Results were compared to two analytical theories developed by *Von-Mises* and *Greiner* for a circular cylinder under hydrostatic pressure and providing the elastic critical buckling pressure.

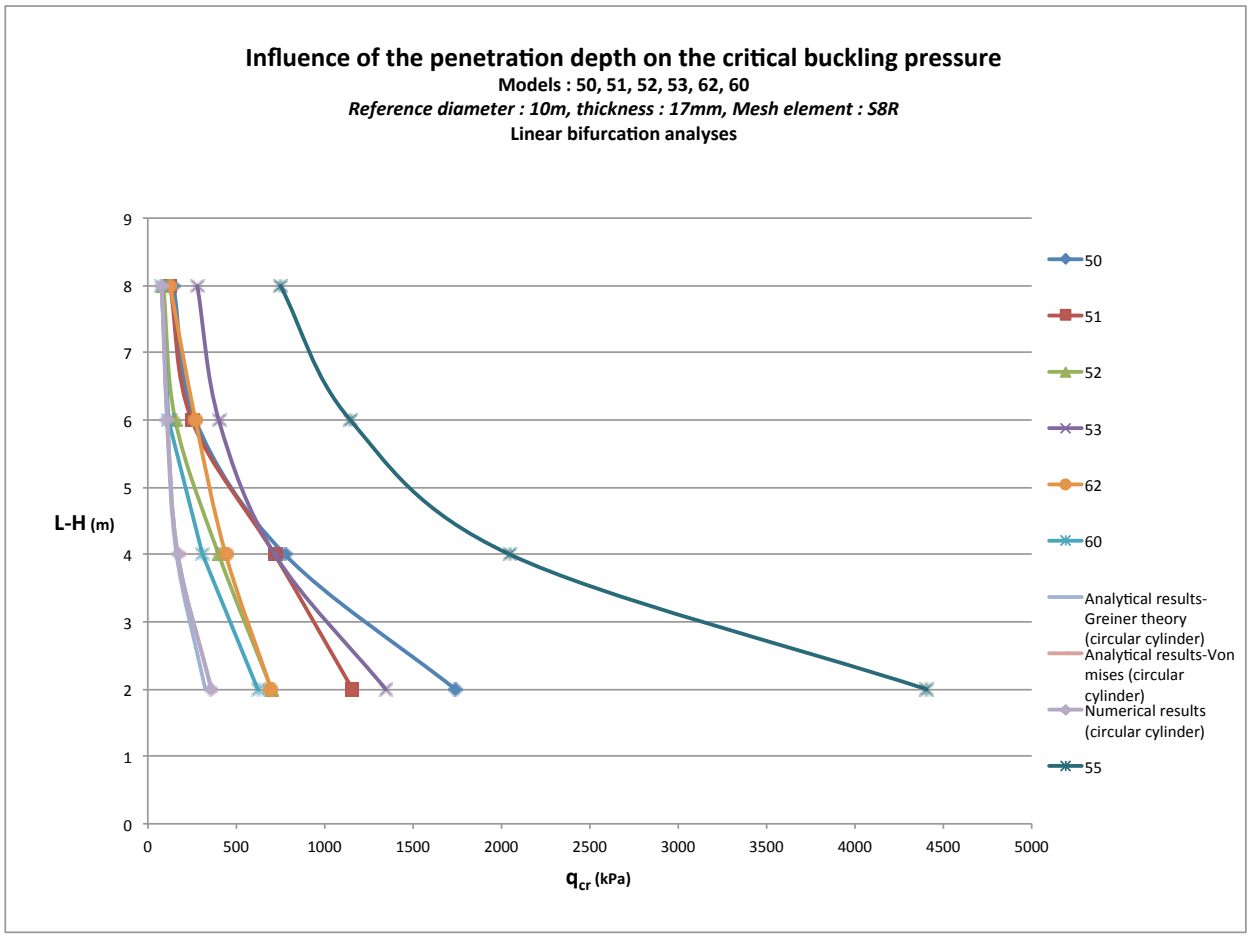

Figure 15 : Linear prediction of the critical buckling pressure for the various shapes for jacket foundation supports as a function of the penetration depth.

Figure 15 emphasizes the strong behaviour provided by shape 55. As a matter of fact, the critical buckling pressures obtained are higher than all the other shapes studied for the support for jacket foundations. The critical buckling load procured for the total length of the suction bucket foundation is q_{cr}*=749 kPa*.

The first buckling mode shape of shape 55 is shown in the Z-X plane on *Figure 39*, Annex B and in 3D on *Figure 51*, Annex C.

5. Nonlinear analyses of the imperfect structure on shape 55

In order to study the real behaviour of the structure, nonlinear analyses were performed. Consequently, the several analyses led to the knockdown factor KDF=0,22 for the enhanced shape 55. This factor was then applied on the predicted results from linear analyses at all the penetration depths studied (*Figure 16*), taking the same approach as it was done for the first shapes drawn.

Even though shape 55 is highly sensitive to imperfections, its behaviour with regards to buckling is still interesting but it is not necessarily the shape providing the best results.

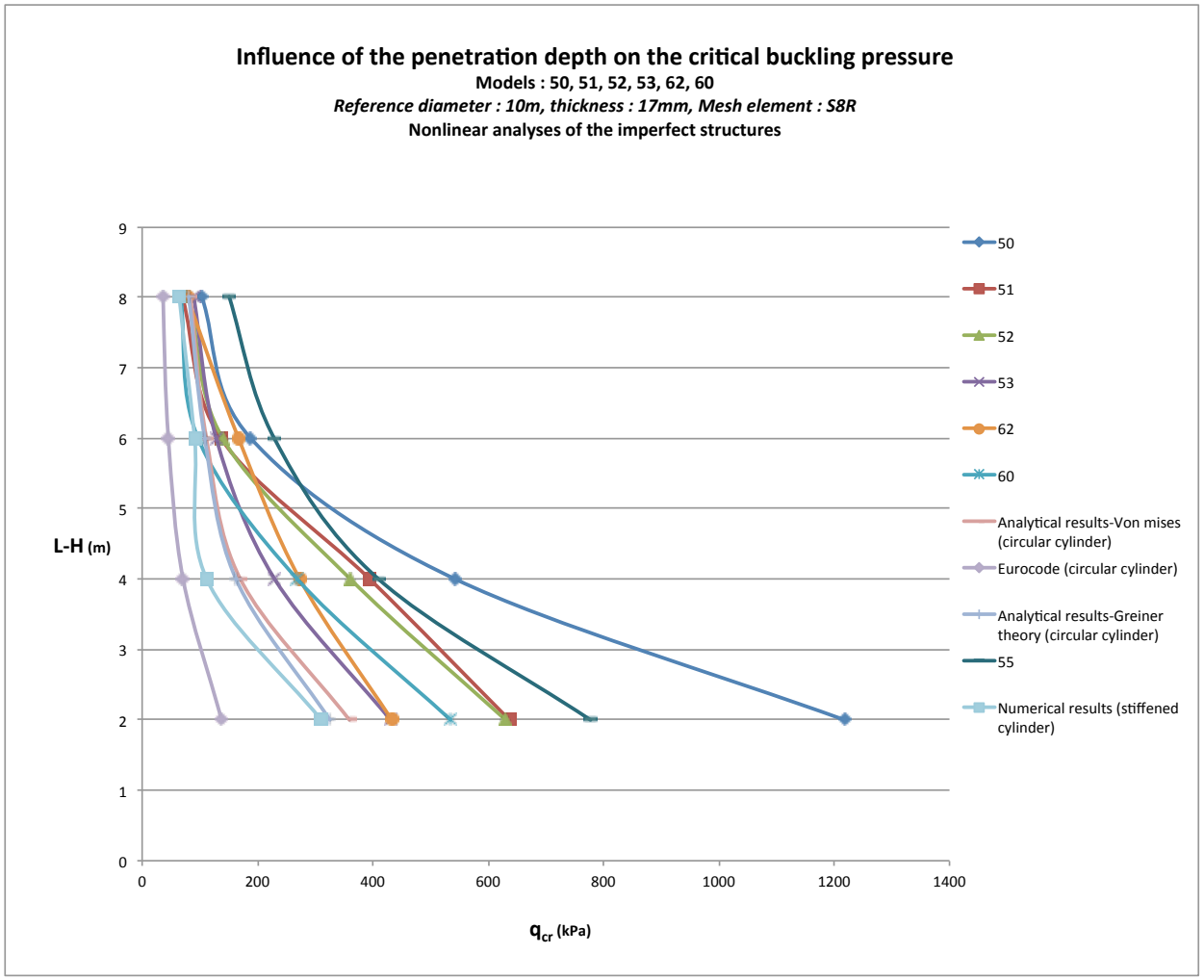

Figure 16 : Nonlinear analyses of the imperfect structure for the various shapes for jacket foundation supports as a function of the penetration depth. The KDF obtained for a bucket foundation length of 8m was applied on each length.

The figure presented above points out the strong behaviour against buckling in the cases of shape 50 and 55. For small penetration depths, the new shape 55 is the strongest one but as soon as the penetration depth reaches half of the length, shape 50 begins to be the more resistant against buckling.

However, other ways to introduce imperfections should be assayed on the different shapes. As a matter of fact, using the buckling shapes from linear results does not obligatorily provide the worst effects on nonlinear analyses.

6. Further investigation regarding Shape 1055 and 55

Shape 1055 for monopod foundations and 55 for support for jacket foundations were chosen to be studied in a more extensive extent. To that extend, numerical analyses were performed on a stiffened circular cylinder with 21 stiffeners for the jacket foundations and 36 stiffeners for the monopod foundations.

The following stiffeners characteristics were selected in accordance with the dimensions chosen previously by Andressen design team for the various enhanced shapes:

- for the monopod foundation:

- Flange thickness: t_{fl}=17mm
- Web thickness: t_{web}=17mm
- Flange width: s_{fl}=120mm
- Height of profile: s_{web}=158mm

- for the jacket foundation:
  - Flange thickness: t_{fl}=17mm
  - Web thickness: t_{web}=17mm
  - Flange width: s_{fl}=120mm
  - Height of profile: s_{web}=161mm

6.1. Linear bifurcation analyses

First of all, the linear predictions for the critical buckling load obtained for the stiffened cylinder were compared to the results provided by the two shapes chosen.
Results shown in *Figure 17* and *Figure 18* enhance that both of the shapes suggested are stronger than a circular cylinder with the same number of stiffeners.

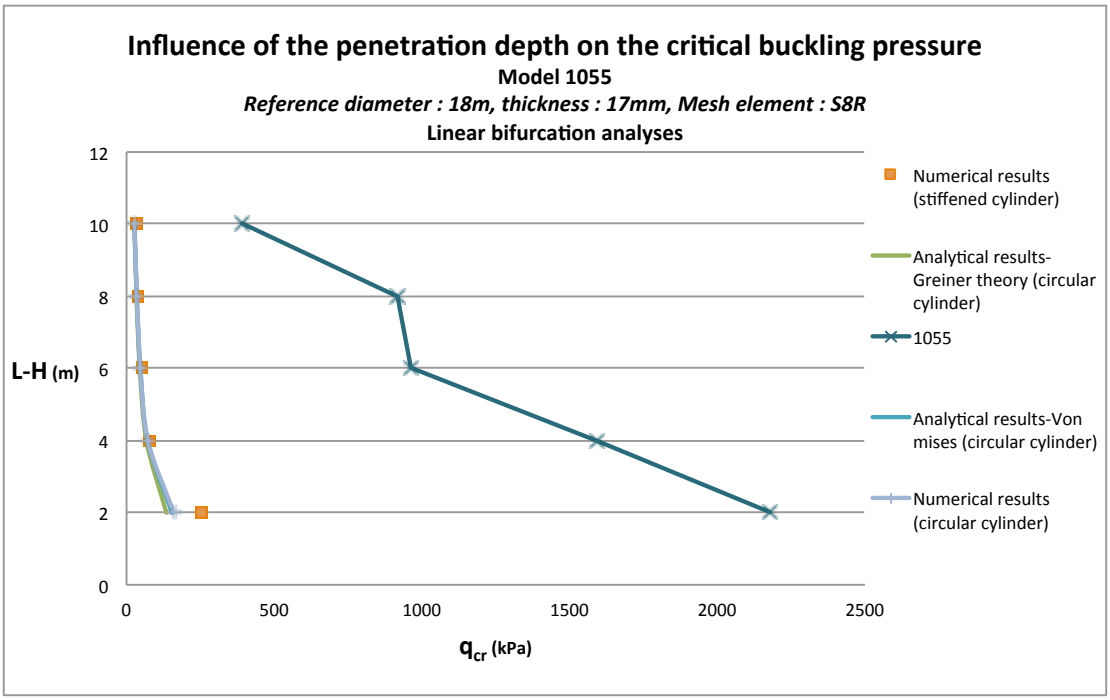

Figure 17 : Linear bifurcation analyses to enhance the buckling behaviour of the monopod foundation respecting to various penetration depths. 36 stiffeners were used on the stiffened circular cylinder.

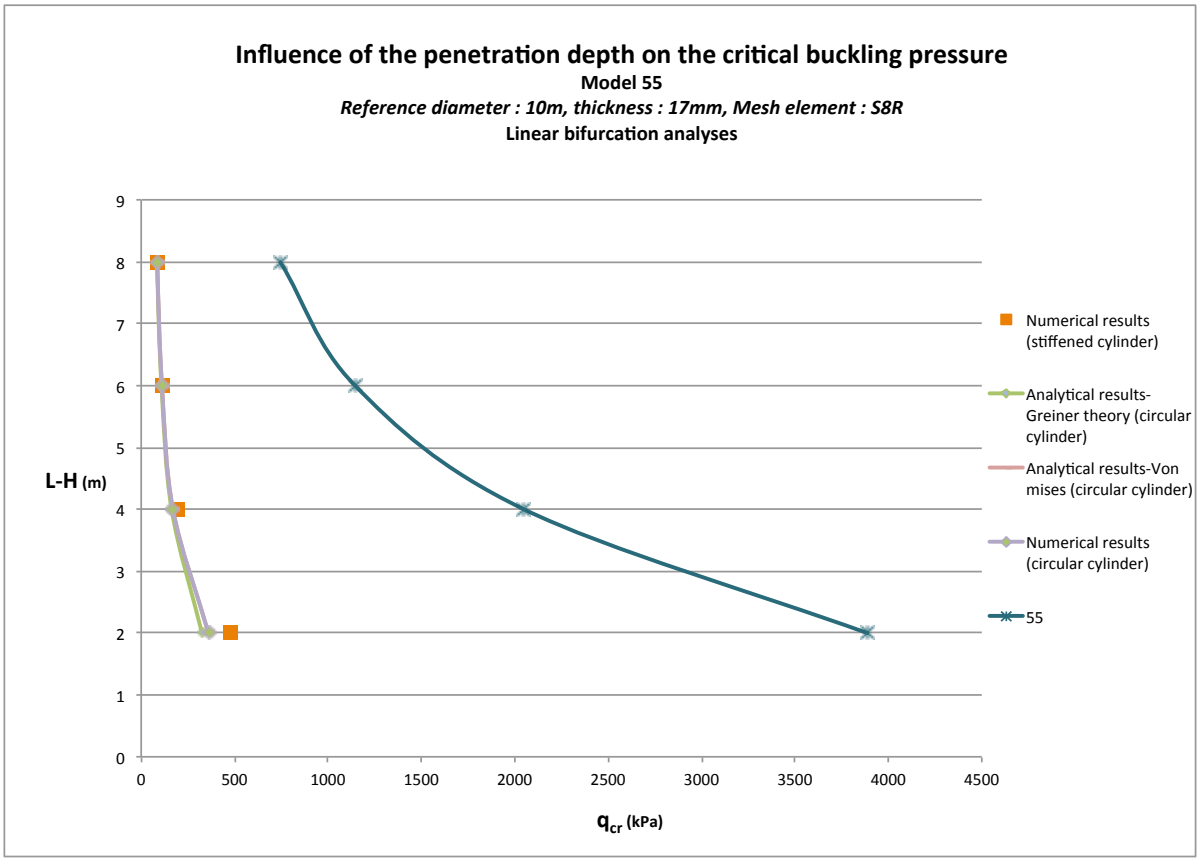

Figure 18 : Linear bifurcation analyses to enhance the buckling behaviour of the support for jacket foundation respecting to various penetration depths. 21 stiffeners were used on the stiffened circular cylinder.

The following figures (*Figure 19* and *Figure 20*) describe the linear behaviour of a circular cylinder with various numbers of stiffeners. A HE300M profile having the following characteristics was arbitrarily chosen:

- Flange thickness: t_{fl}=39mm
- Web thickness: t_{web}=21mm
- Flange width: s_{fl}=310mm
- Height of profile: s_{web}=340mm

A particular behaviour can be seen when the number of stiffeners is 18 for the monopod foundation and 12 for the jacket foundation. These stiffeners numbers provide a higher critical buckling load than the one obtained for the surrounding values.

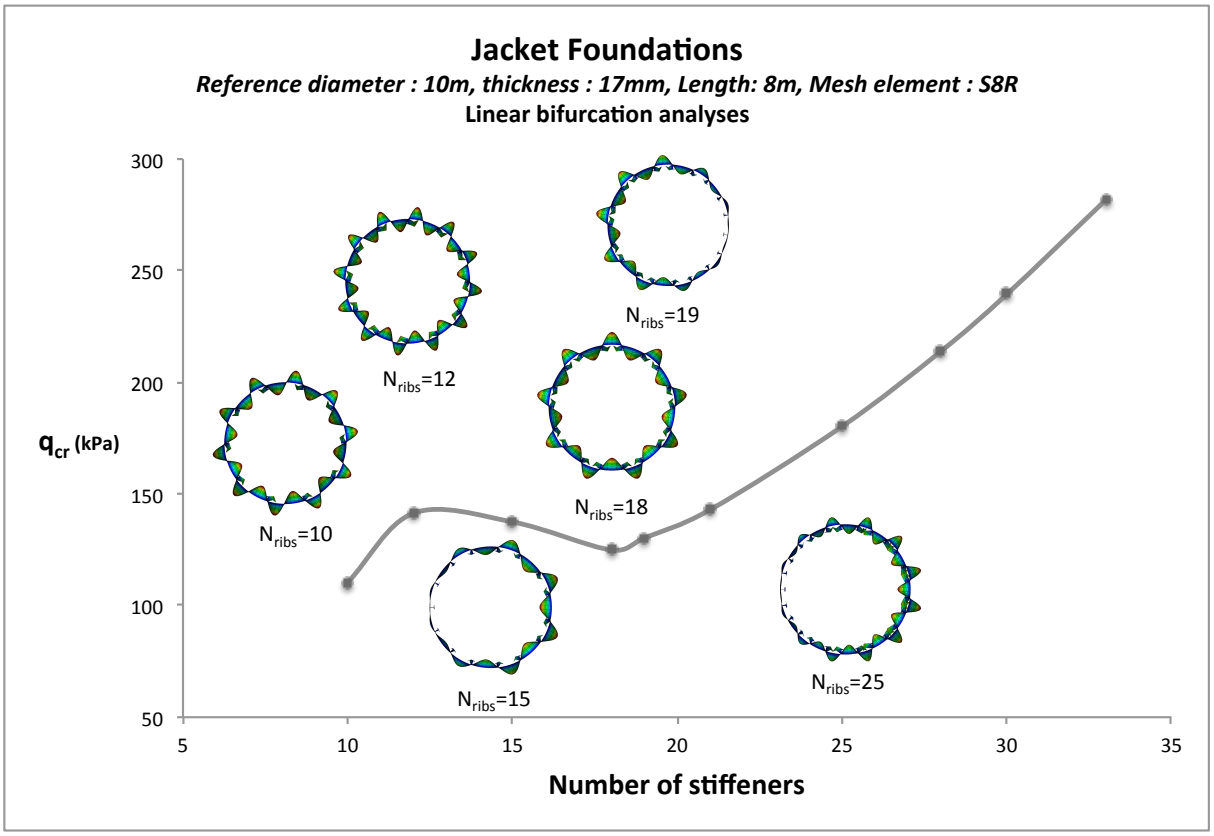

Figure 19 : Critical buckling load as a function of the number of stiffeners for a stiffened circular cylinder with the jacket foundation reference dimensions.

Figure 19 shows that for higher number of ribs (N_{ribs}), the critical buckling mode is unsymmetrical. On the other hand, for a lower number of ribs, changes between symmetrical and unsymmetrical mode shapes are procuring non-linear variation of the critical buckling load.

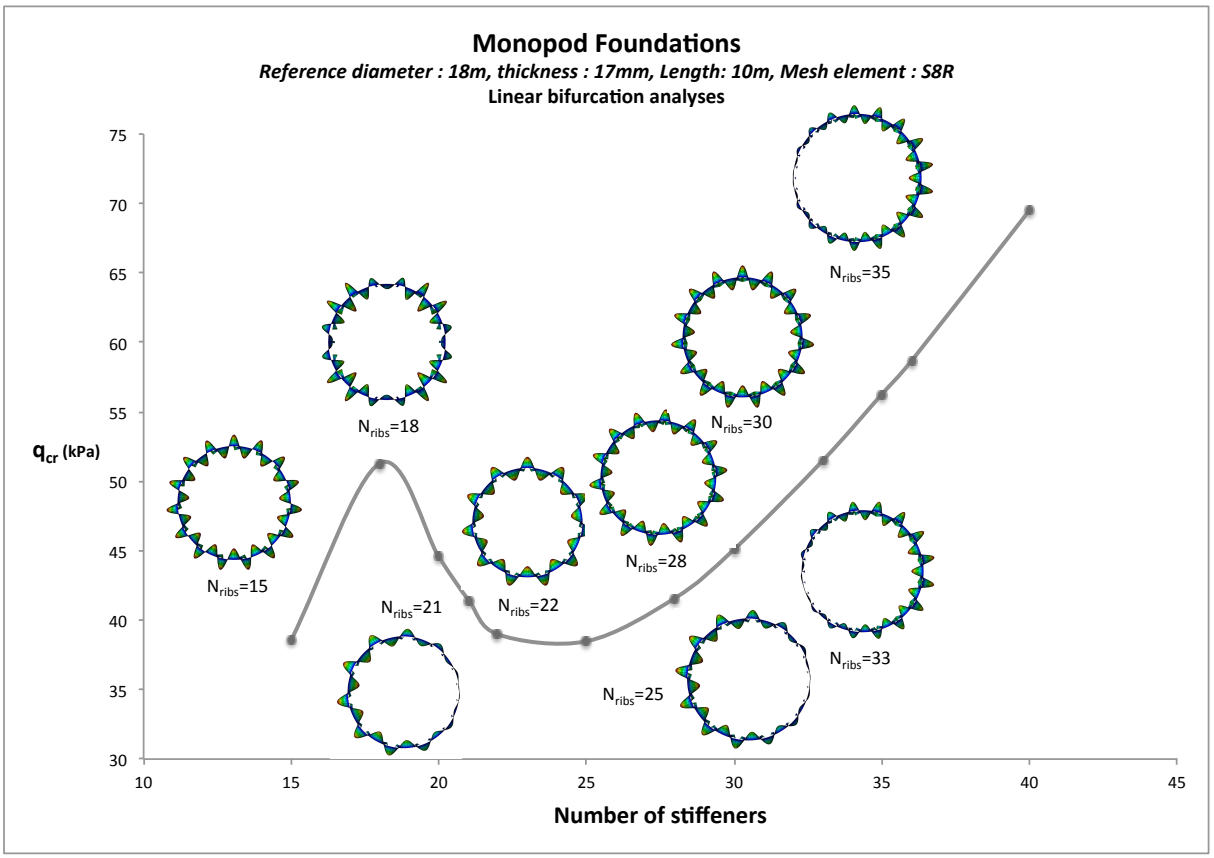

Figure 20 :Critical buckling load as a function of the number of stiffeners for a stiffened circular cylinder with the monopod foundation reference dimensions.

Unlike for the jacket foundations, no general pattern regarding the influence of the number of ribs on the critical buckling mode shape of a stiffened circular cylinder with monopod foundations dimensions can be seen on *Figure 20*.

However, the HE300M profile is a strong profile. Thus, the critical buckling pressure was sought for various standard profiles presented in *Table 3* to place the HE300M behaviour but also of the non-standardised profile chosen for the comparison with the enhanced shapes behaviour. The monopod foundation dimensions were used and 36 stiffeners were considered.

Table 3 : Profiles section characteristics.

profile type	IPN			HEB			HEA			HEM		
profile number	320	360	500	240	300	400	360	400	450	200	240	300
I_x (cm^4)	12510	19610	68740	11260	25170	57680	33090	45070	63720	10640	24290	59200
t_w (mm)	11,5	13	18	10	11	13,5	10	11	11,5	15	18	21
t_f (mm)	17,3	19,5	27	17	19	24	17,5	19	21	25	32	39
b (mm)	131	143	185	240	300	300	300	300	300	206	248	310
h (mm)	320	360	500	240	300	400	350	390	440	220	270	340

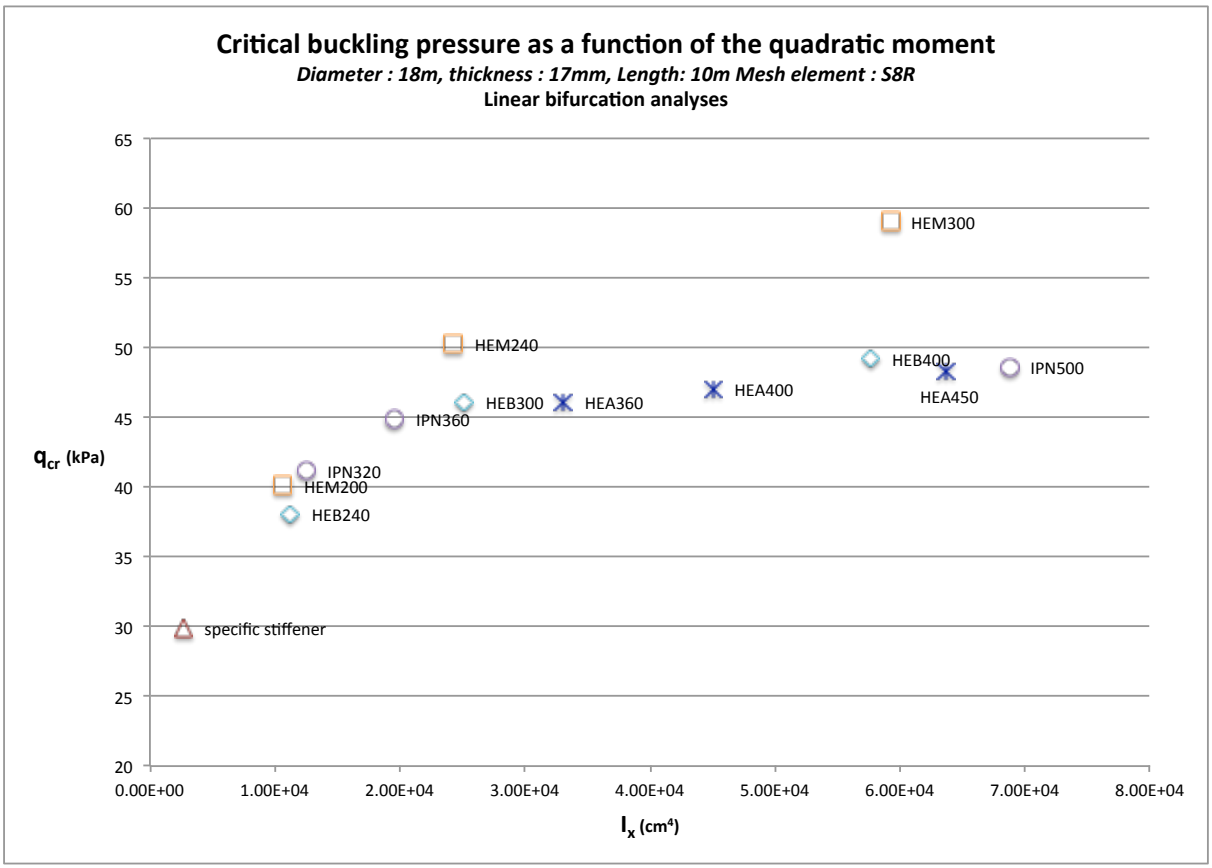

Figure 21 : Critical buckling pressure as a function of the quadratic moment of the major axis for several standard profile sections and for the non-standardised profile section used.

Figure 21 shows the linear buckling pressure as a function of the quadratic moment of the strongest axis I_x for several profiles. As expected, the HEM300 is highly resistant against buckling and other sections like HEM200, IPN320 and HEB240 would be more realistic to be used on a 17mm thickness cylinder.

6.2. Geometrically and materially nonlinear analyses of the imperfect structure

Nonlinear analyses were performed to study the real behaviour of the structure. To be more precise, a knockdown factor was obtained for each foundation length using the corresponding first buckling mode shape.
These results were compared to the ones provided by the stiffened circular cylinder on which various knockdown factors were applied for each cylinder length.

The first buckling mode shape was introduced as an imperfection. Other ways to introduce imperfection were investigated to see if more unfavourable results could be obtained: a point load and an imposed displacement. Nonetheless, the first buckling mode shape was providing the most accurate results.

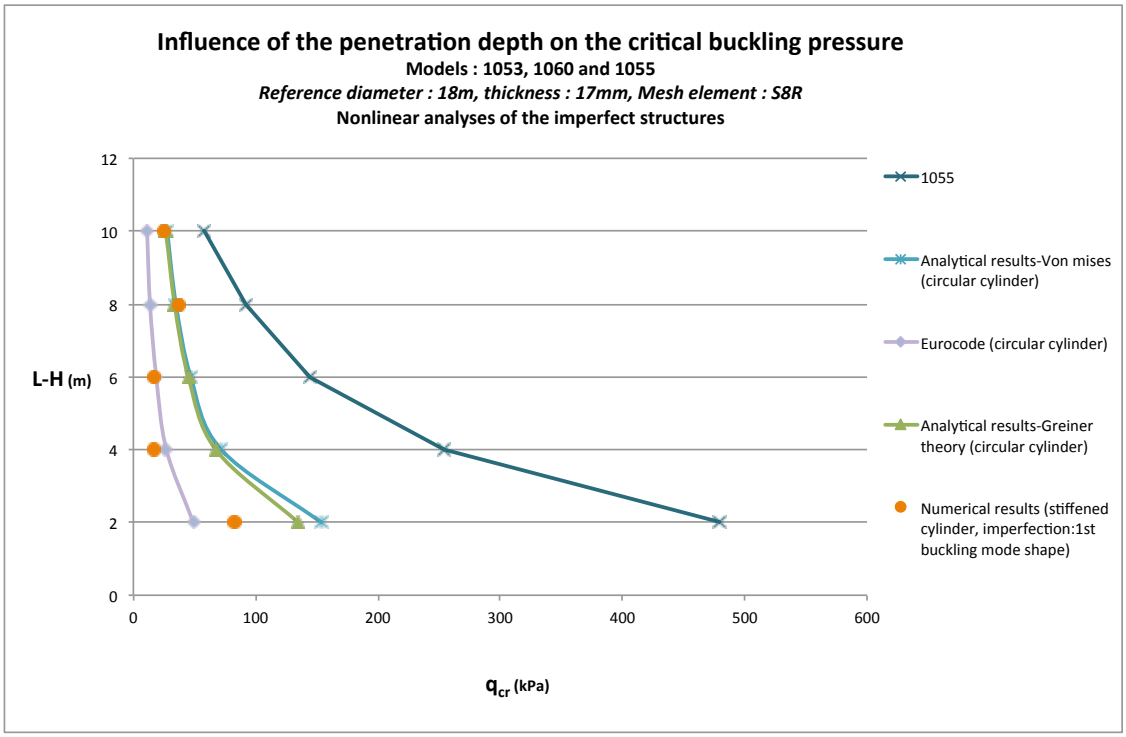

Figure 22 : Nonlinear analyses of the imperfect structure for the various shapes for monopod foundations as a function of the penetration depth. The KDF obtained for each length was applied. The stiffened circular cylinder considered included 36 stiffeners.

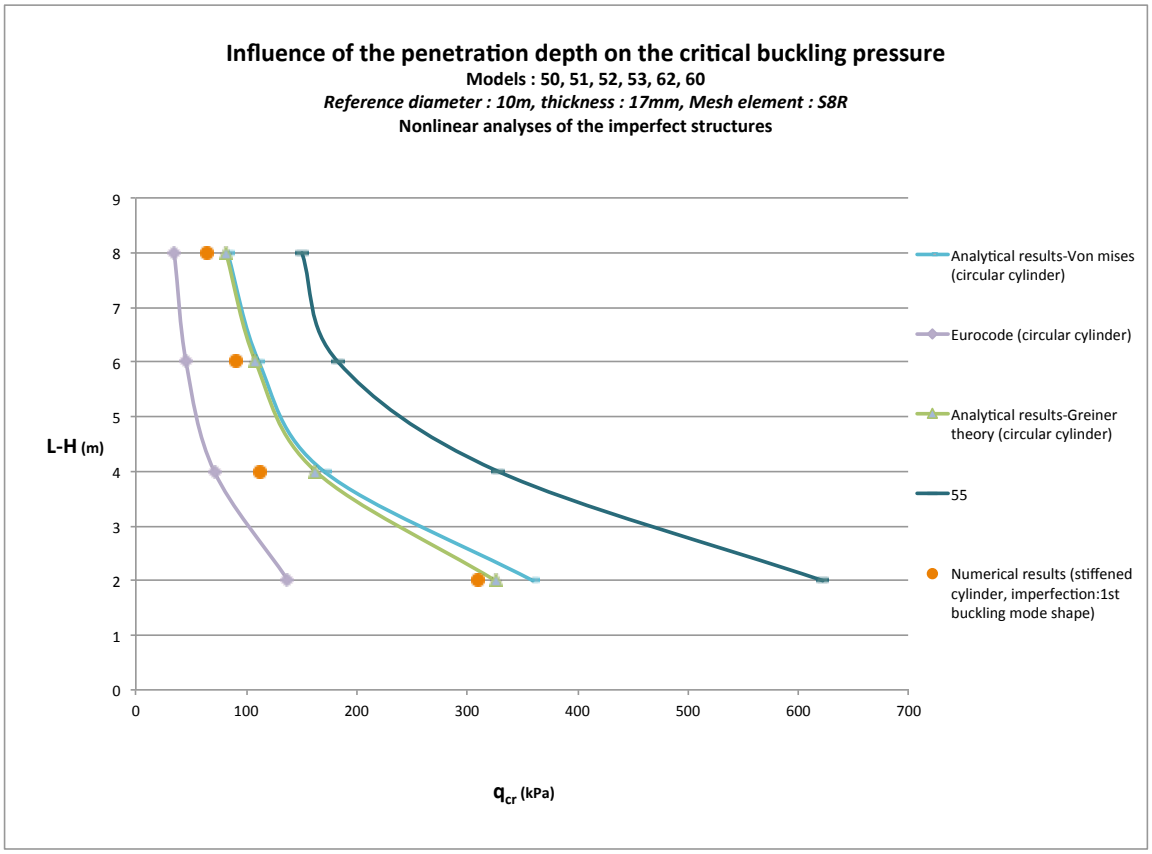

Figure 23 : Nonlinear analyses of the imperfect structure for the various shapes for jacket foundation supports as a function of the penetration depth. The KDF obtained for each length was applied. The stiffened circular cylinder considered included 21 stiffeners.

Results presented on *Figure 22* and *Figure 23* point out that both of the shapes 1055 and 55 are still stronger against buckling than a stiffened circular cylinder when non-linearity is considered.

7. Conclusion

The enhanced shapes 55 for the supports for jacket foundations and 1055 associated to monopod foundations seem to be reliable regarding their buckling behaviour. As a matter of fact, taking into account the results obtained from linear and non-linear analyses, these shapes provide a stronger resistance than a circular cylinder and than a stiffened circular cylinder with adequate stiffeners.

The several panels were considered as entirely fixed between each other. Thus, further investigation respecting the mechanical behaviour of the junction between the several panels should be carried out.

Appendices

A. EUDP project/ Suction bucket foundation shapes

IB ANDRESEN INDUSTRI

Design typer på Sugebøtter, 18/6-2016 Arne Kryger

Jacket buckets:

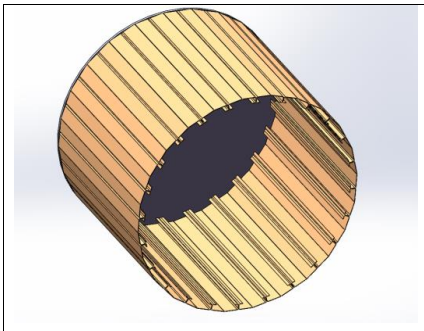	Type 50 Ø10meter 24 segmenter L=8000mm Dobbelt ombuk. begge sider
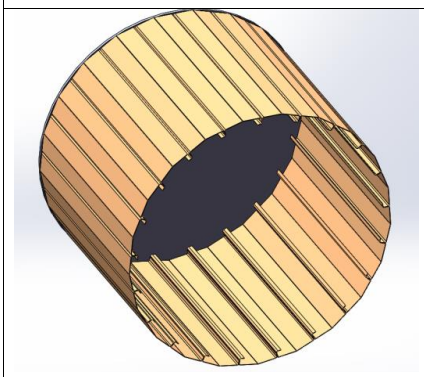	Type 51 Ø10meter 21 segmenter L=8000mm Dobbelt ombuk, den ene side
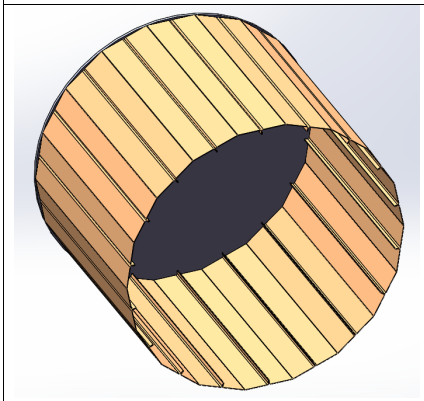	Type 52 Ø10meter 18 segmenter L=8000mm Ingen ekstra buk

Figure 24 : Suction bucket foundation designs 50 to 52.

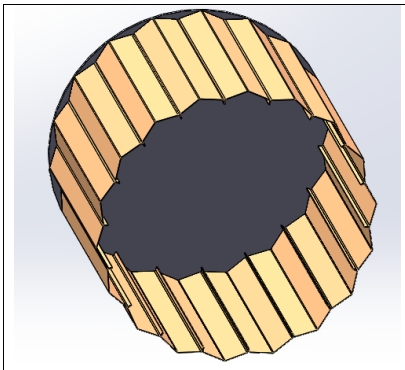	Type 53 Ø10meter 18 segmenter L=8000mm ”Cookie cutter” Større stivhed i hvert segment
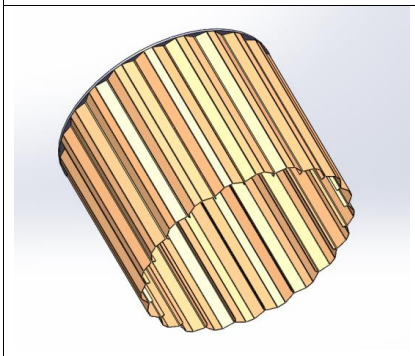	Type 55 Ø10meter 21 segmenter L=8000mm ”Cookie cutter” Ekstra buk på segmenter
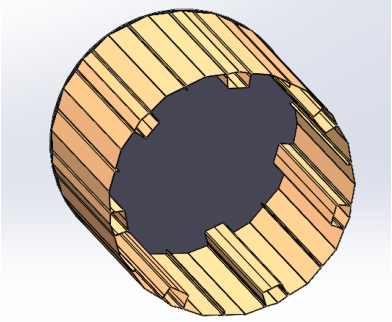	Type 60 Ø10meter 14 segmenter + 7 lukkede rør L=8000mm

Figure 25 : Suction bucket foundation designs 53 to 60.

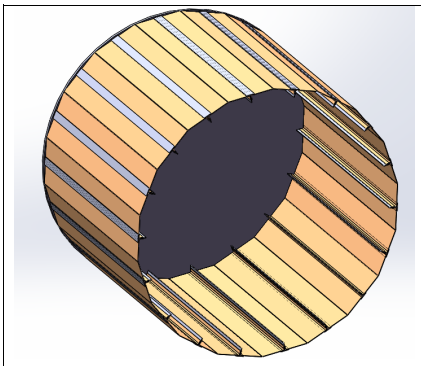	Type 62 Ø10meter 18 segmentet + 18 T-profiler L=8000mm
Mono buckets:	
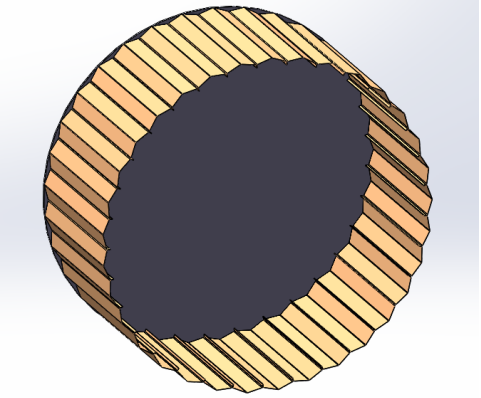	Type 1053 Ø18meter 33 segmenter L=10000mm ”Cookie cutter” Større stivhed i hvert segment

Figure 26 : Suction bucket foundation designs 62 and 1053.

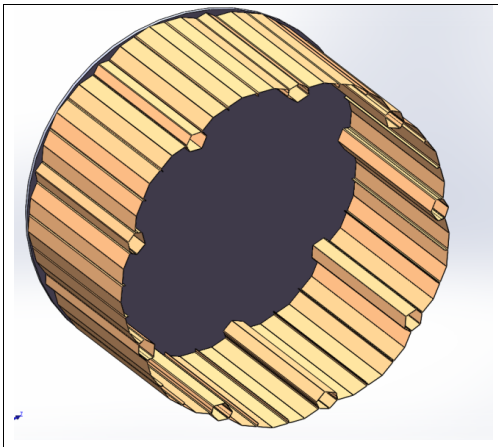	Type 1060 Ø18meter 27 segmenter + 9 lukkede rør L=10000mm ”Flower shape”
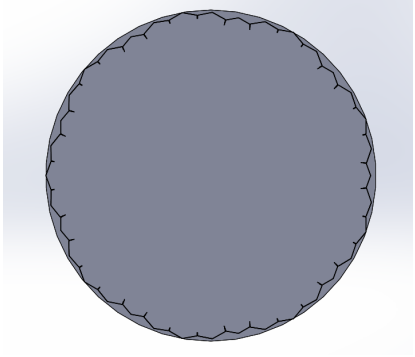	Type 1054 Ø18meter 27 + 9 segmenter L=10000mm “Flower shape + Cookie cutter”
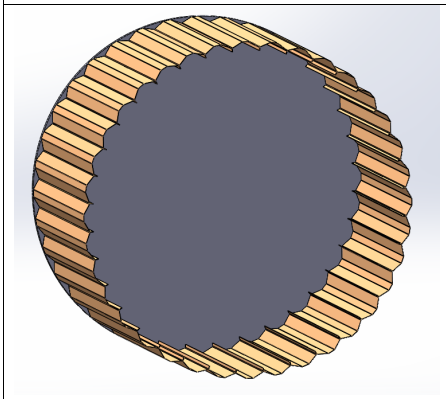	Type 1055 Ø18meter 36 segmenter L=10000mm ”Cookie cutter” Ekstra buk på segmenter

Figure 27 : Suction bucket foundation shape 1060 to 1055.

B. EUDP Project/ first step, Buckling shapes (Z-X) plane

The first mode shape is shown for all of the figures.

- **Model 1053, length: 10m**

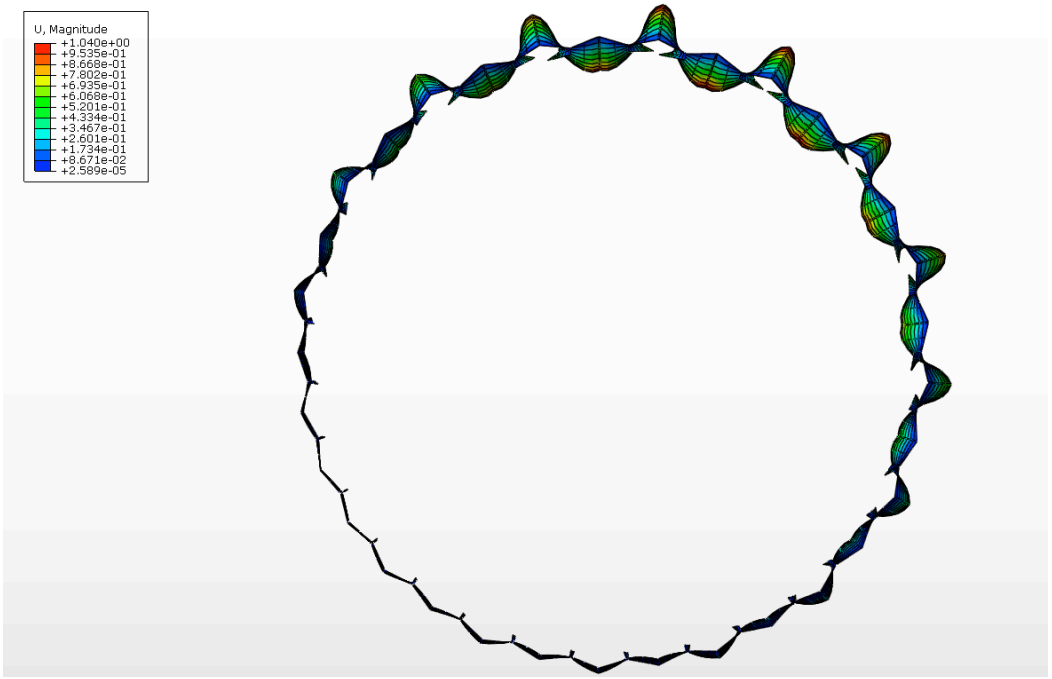

Figure 28 : Model 1053, Buckling shape in the (Z-X) plane.

- **Model 1060, length: 10m**

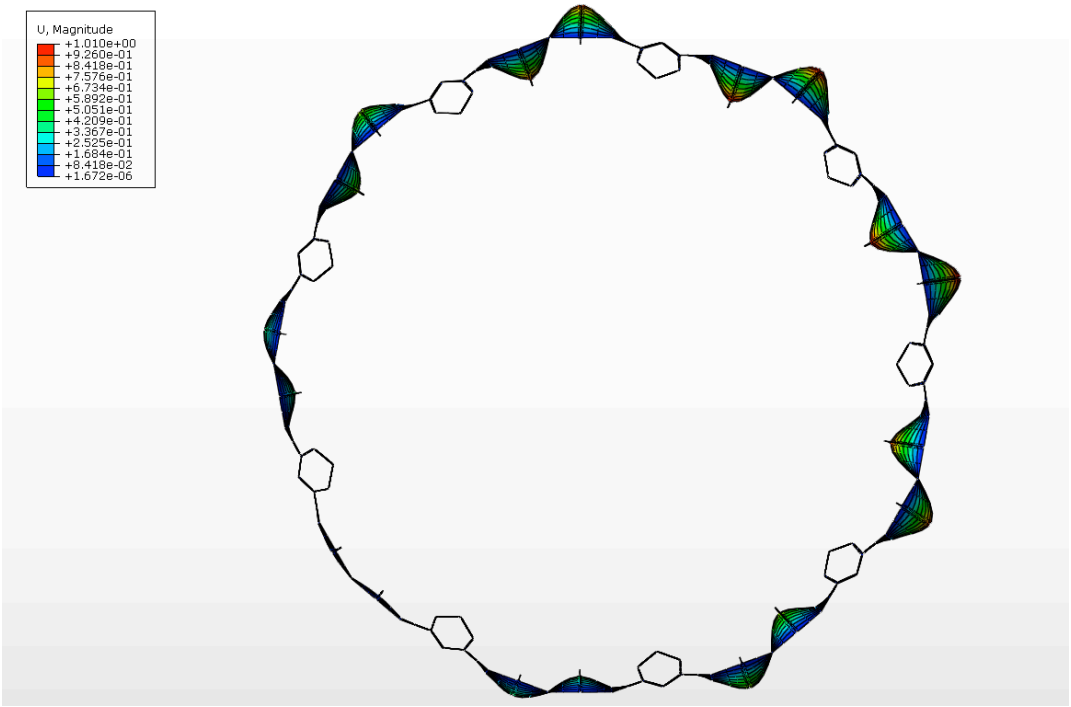

Figure 29 : Model 1060, Buckling shape in the (Z-X) plane.

- **Model 50, length: 8m**

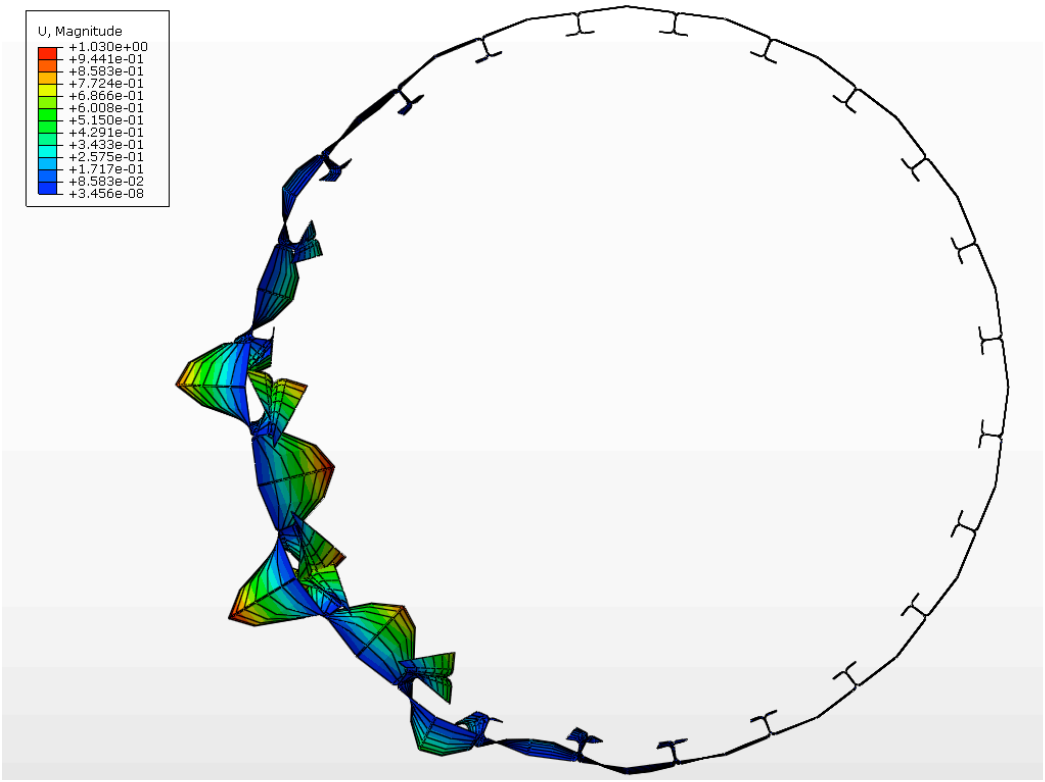

Figure 30 : Model 50, Buckling shape in the (Z-X) plane.

7.1. Model 51, length: 8m

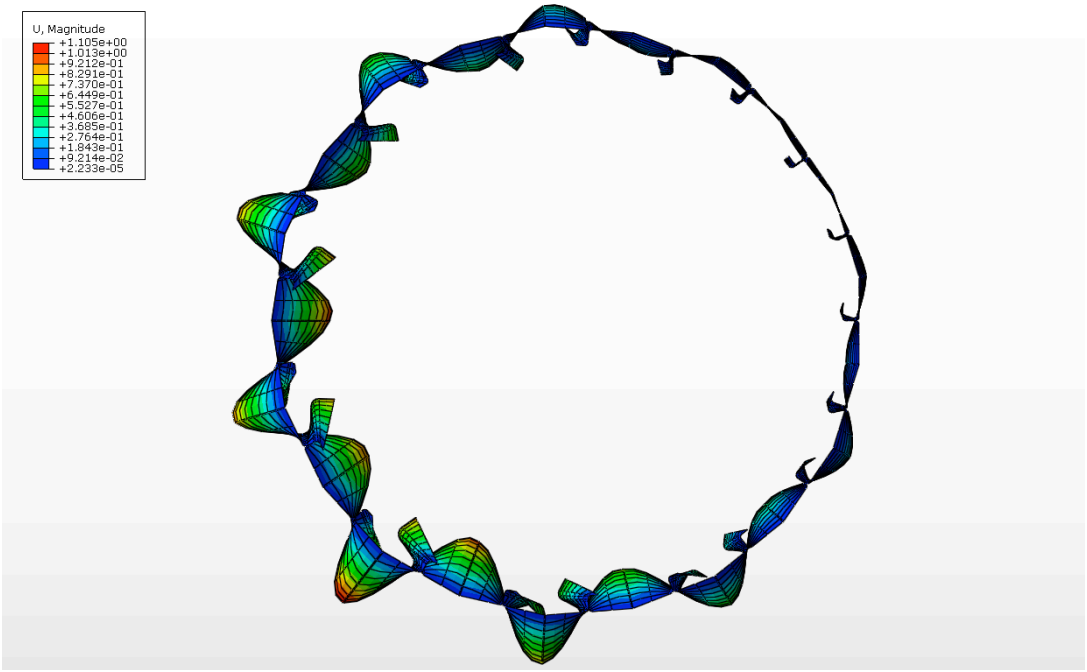

Figure 31 : Model 51, Buckling shape in the (Z-X) plane.

- **Model 52, length: 8m**

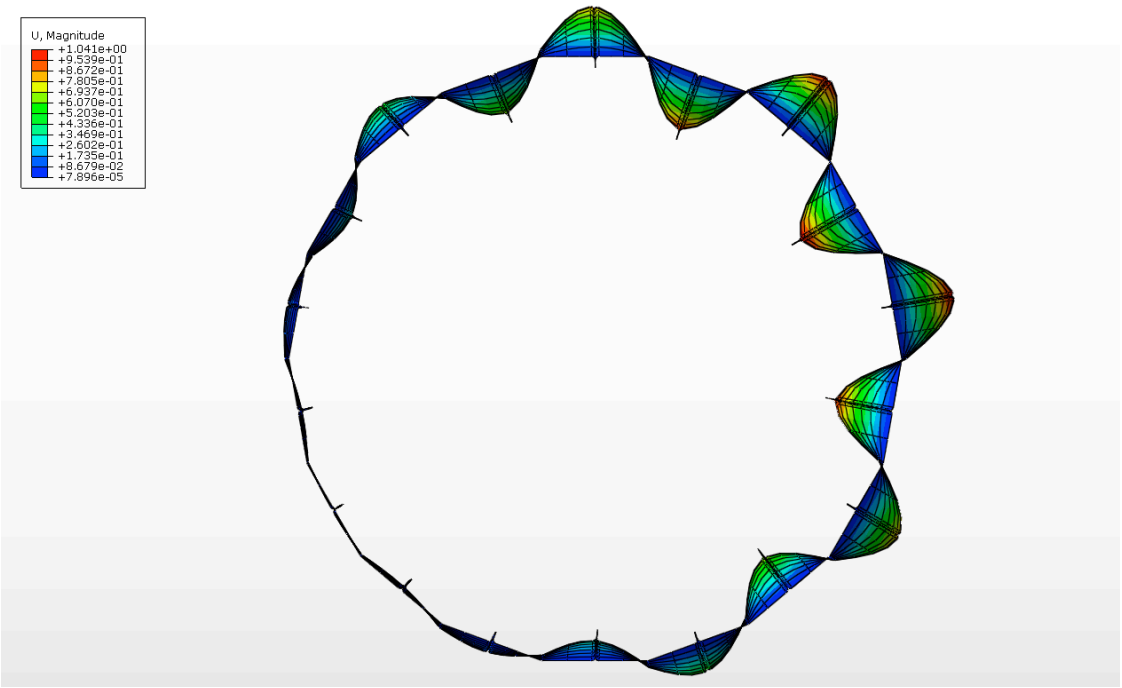

Figure 32 : Model 52, Buckling shape in the (Z-X) plane.

- **Model 53, length: 8m**

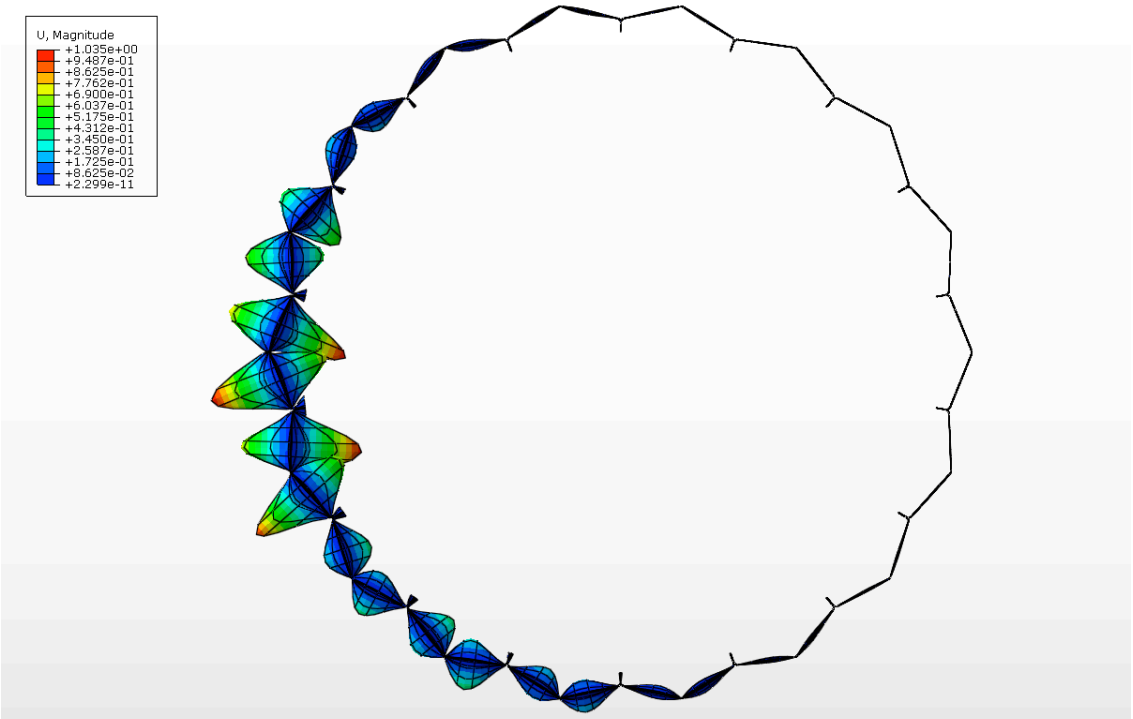

Figure 33 : Model 53, Buckling shape in the (Z-X) plane.

- **Model 60, length: 8m**

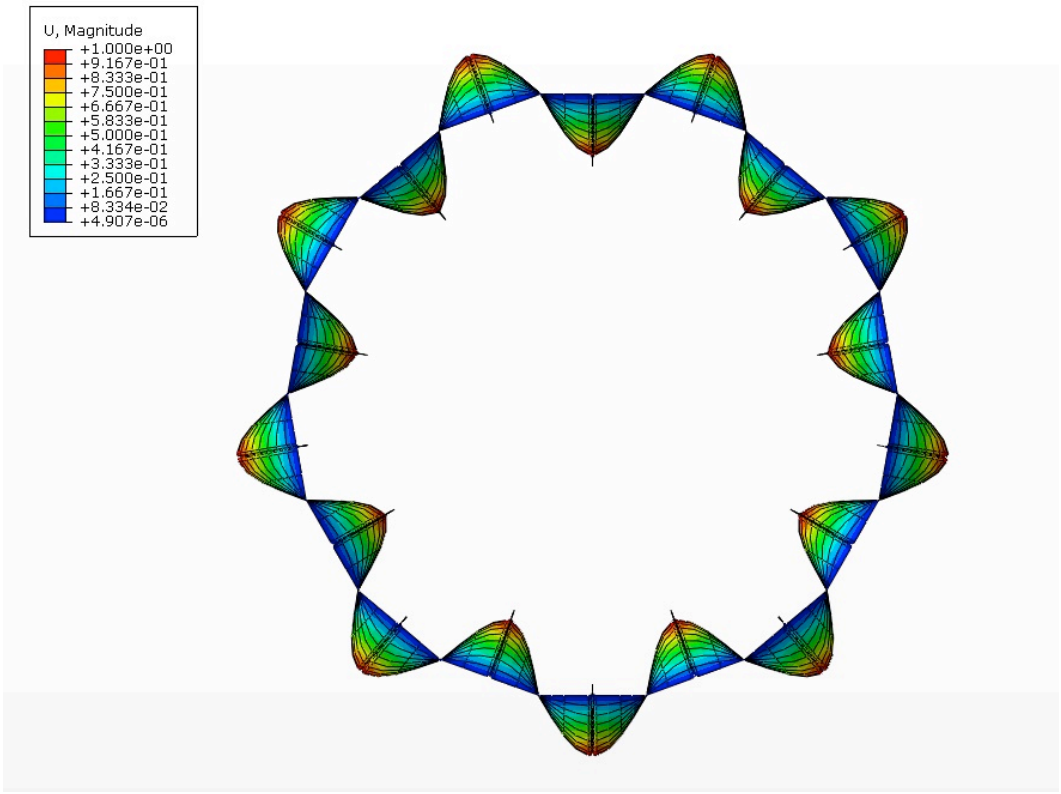

Figure 34 : Model 60, Buckling shape in the (Z-X) plane.

- **Model 62, length: 8m**

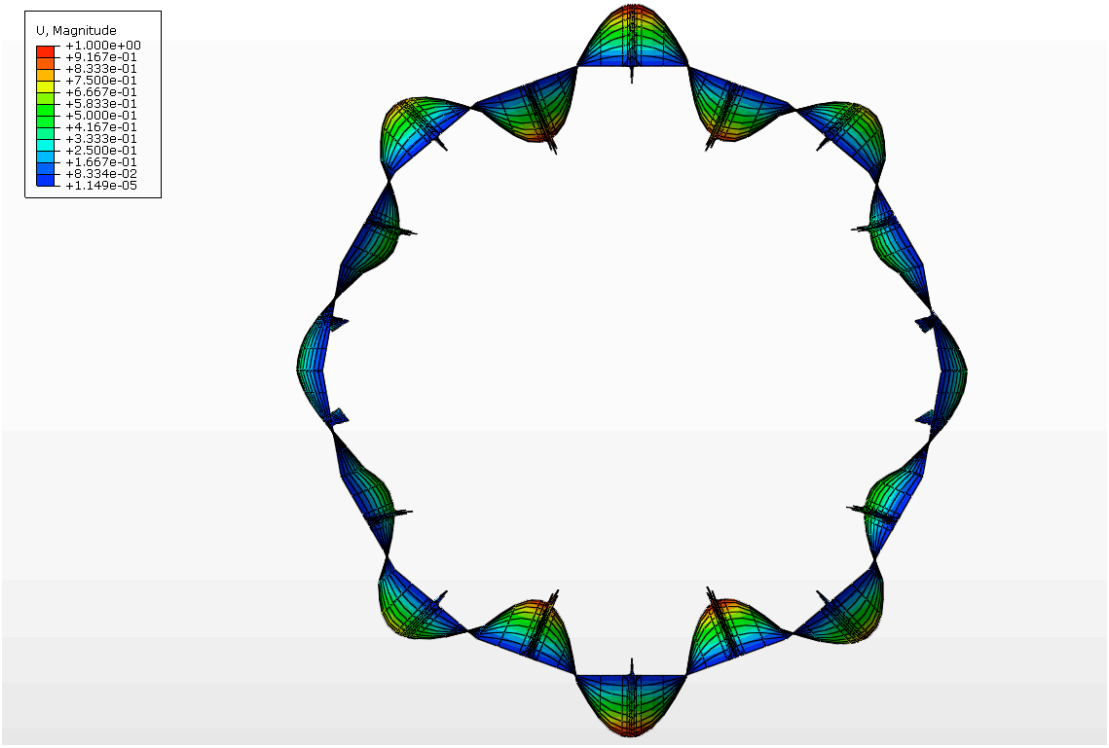

Figure 35 : Model 62, Buckling shape in the (Z-X) plane.

- **Model 1055, length: 10m**

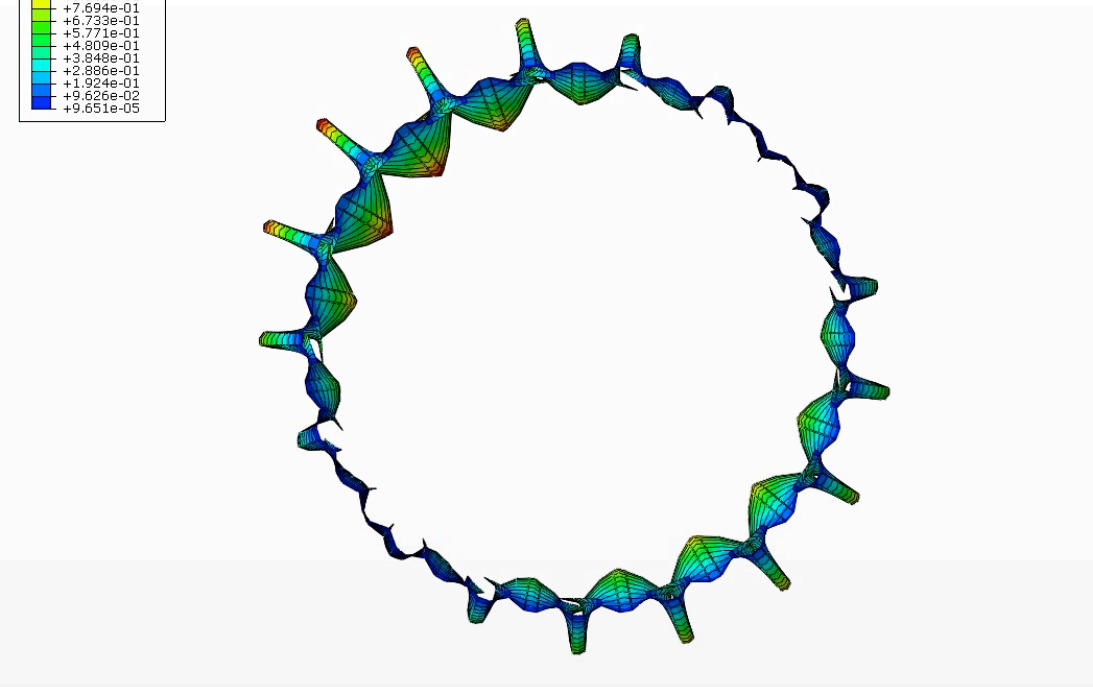

Figure 36 : Model 1055, Buckling shape in the (Z-X) plane.

- **Model 1055, length: 8m**

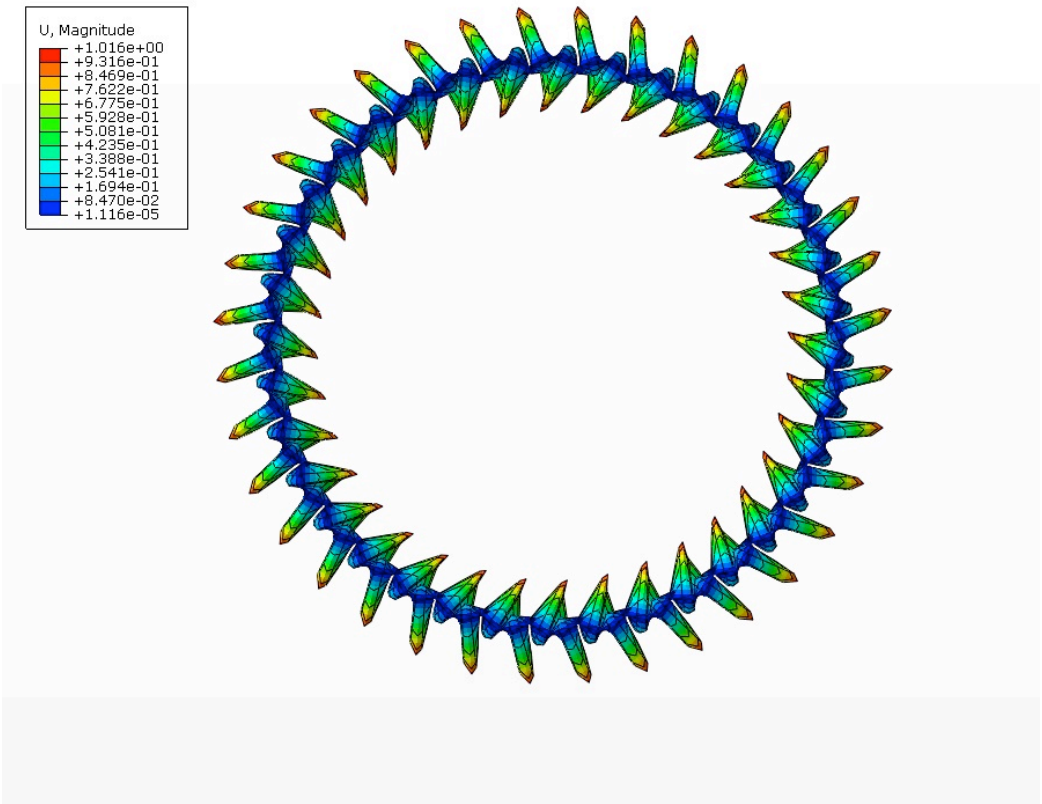

Figure 37 : Model 1055 (length:8m), Buckling shape in the (Z-X) plane.

- **Model 1055, length: 6m**

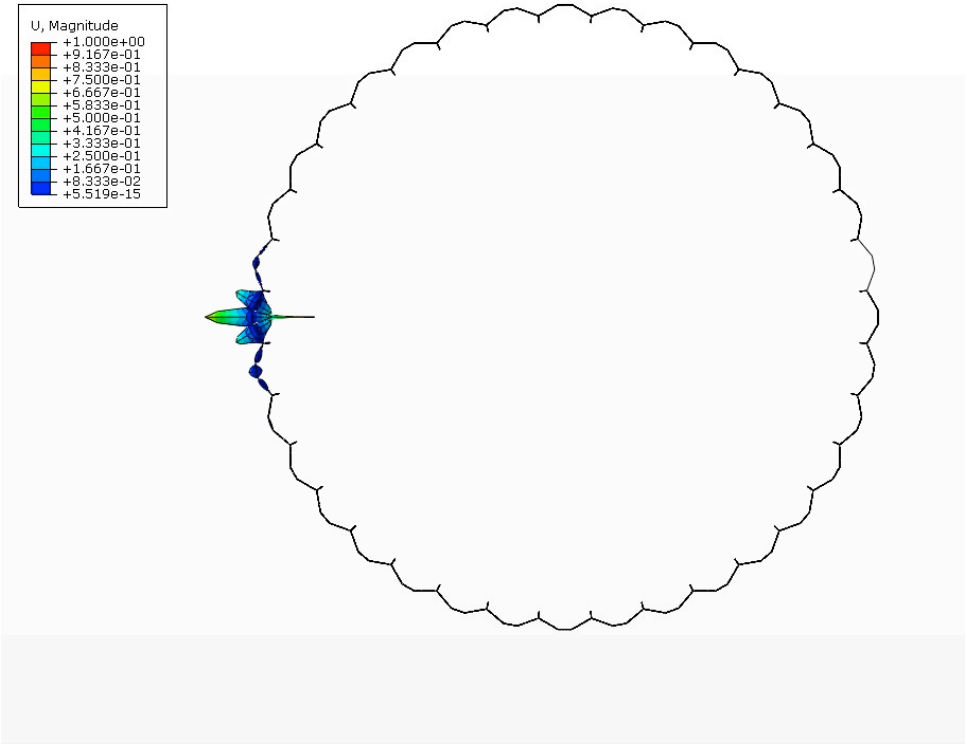

Figure 38 : Model 1055 (length:6m), Buckling shape in the (Z-X) plane.

- **Model 55, length: 8m**

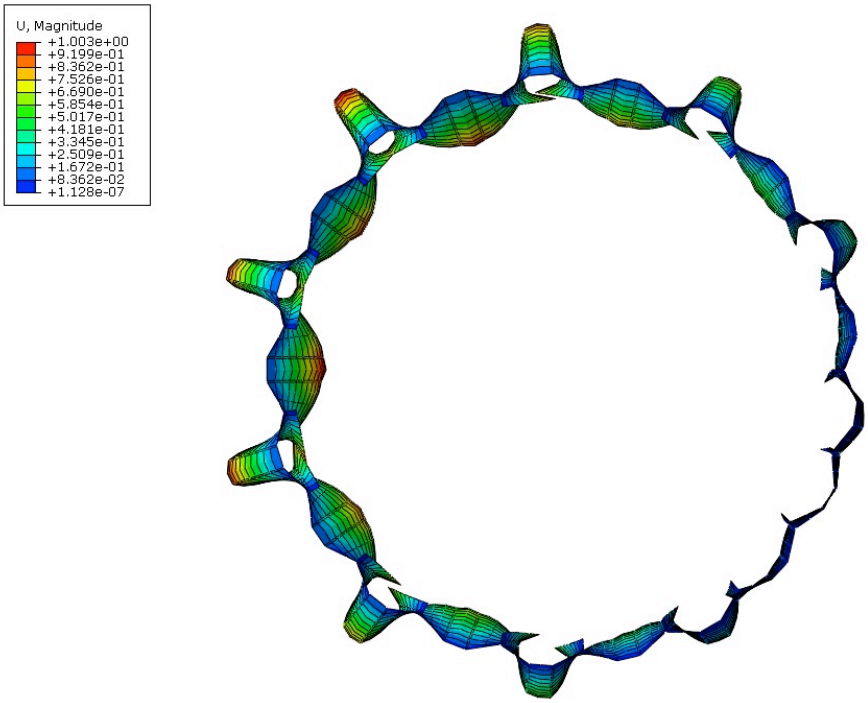

Figure 39 : Model 55, Buckling shape in the (Z-X) plane.

C. EUDP Project/ first step, Buckling shapes (3D)

The first mode shape is shown for all of the figures.

- **Model 1053, length: 10m**

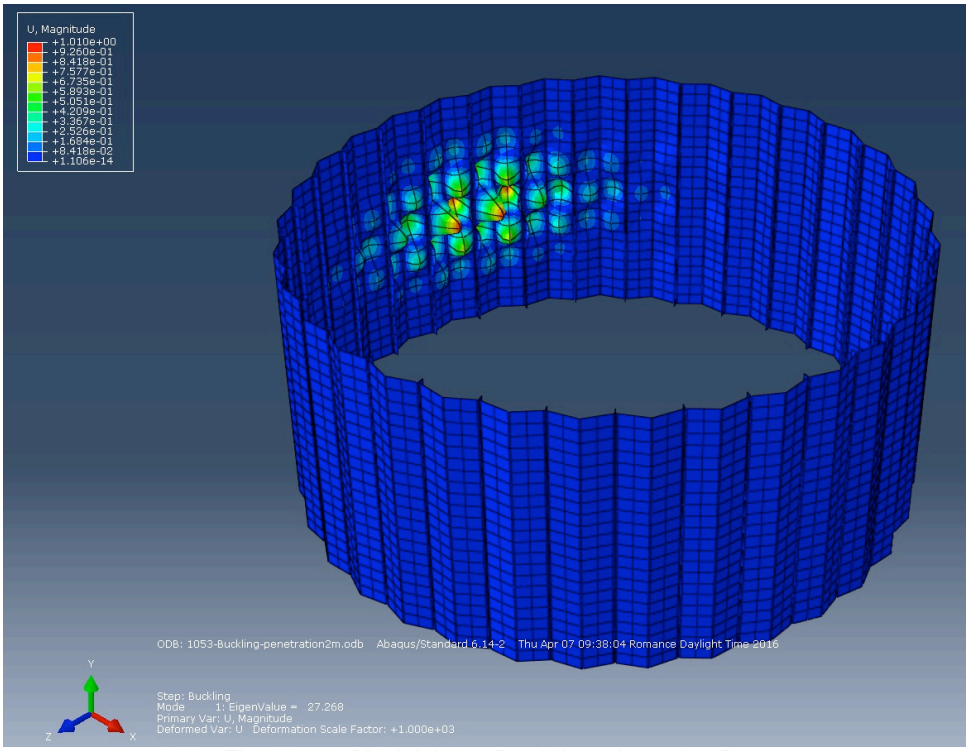

Figure 40 : Model 1053, Buckling shape in 3D.

- **Model 1060, length: 10m**

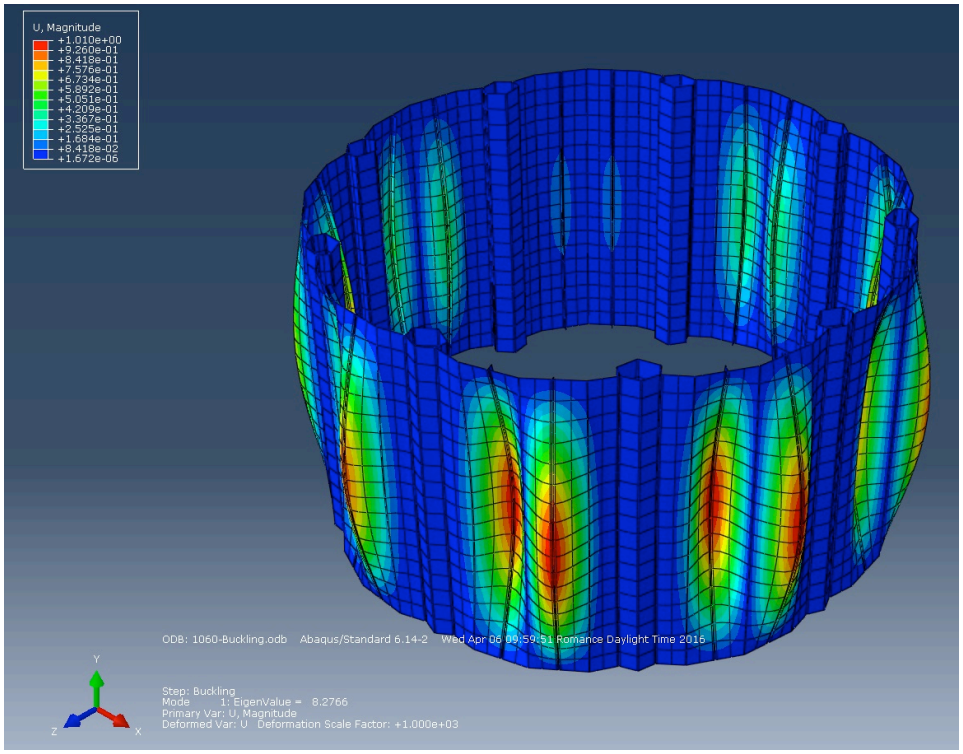

Figure 41 : Model 1060, Buckling shape in the 3D.

- **Model 50, length: 8m**

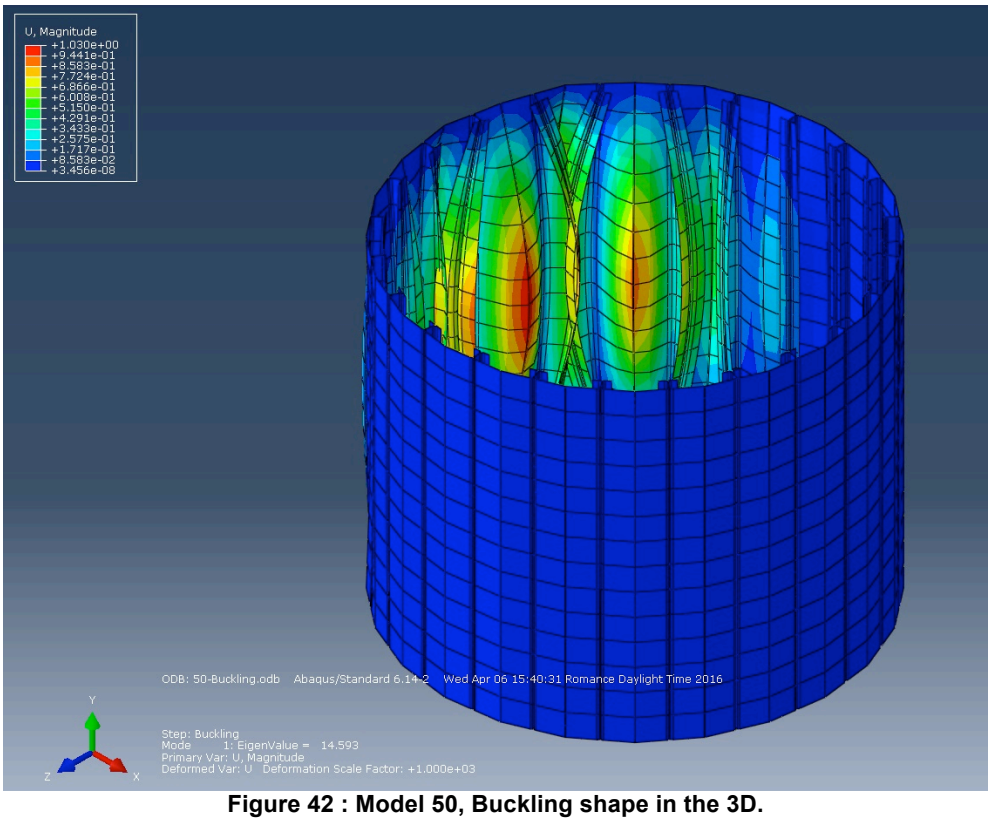

Figure 42 : Model 50, Buckling shape in the 3D.

- **Model 51, length: 8m**

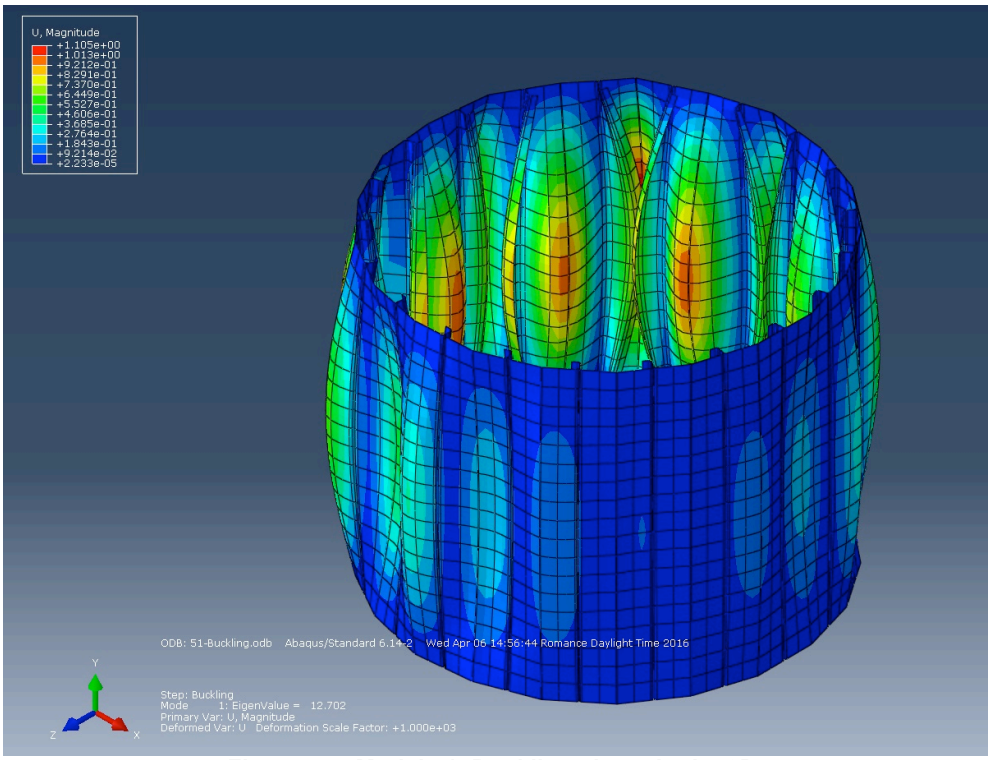

Figure 43 : Model 51, Buckling shape in the 3D.

- **Model 52, length: 8m**

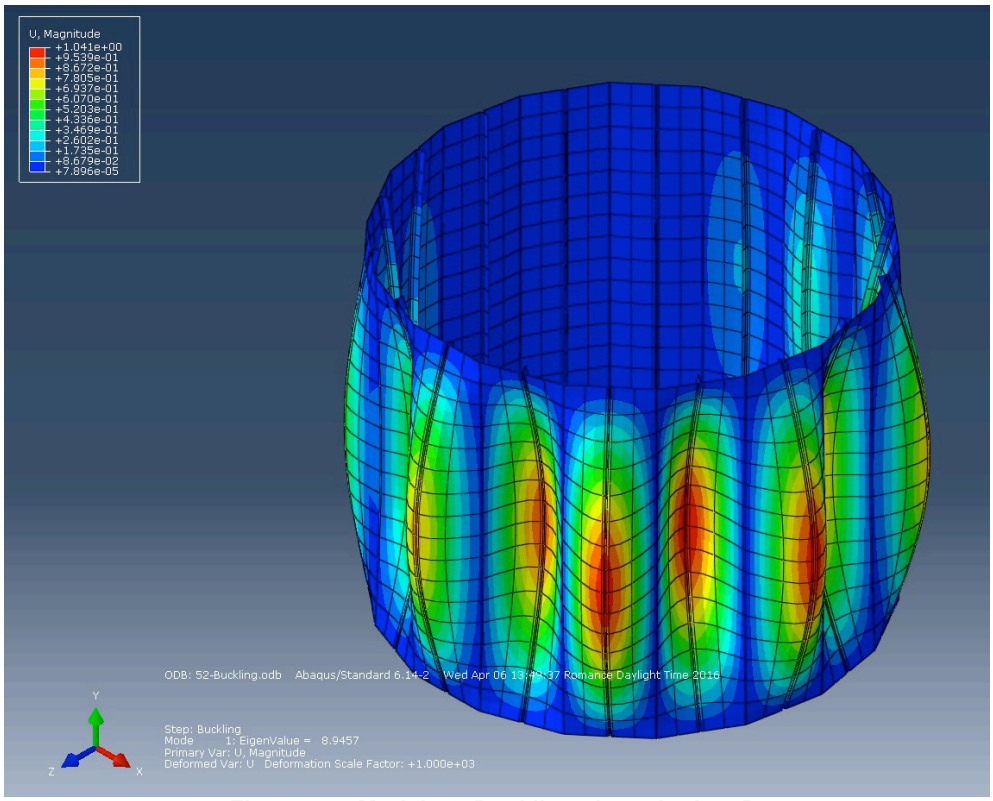

Figure 44 : Model 52, Buckling shape in the 3D.

- **Model 53, length: 8m**

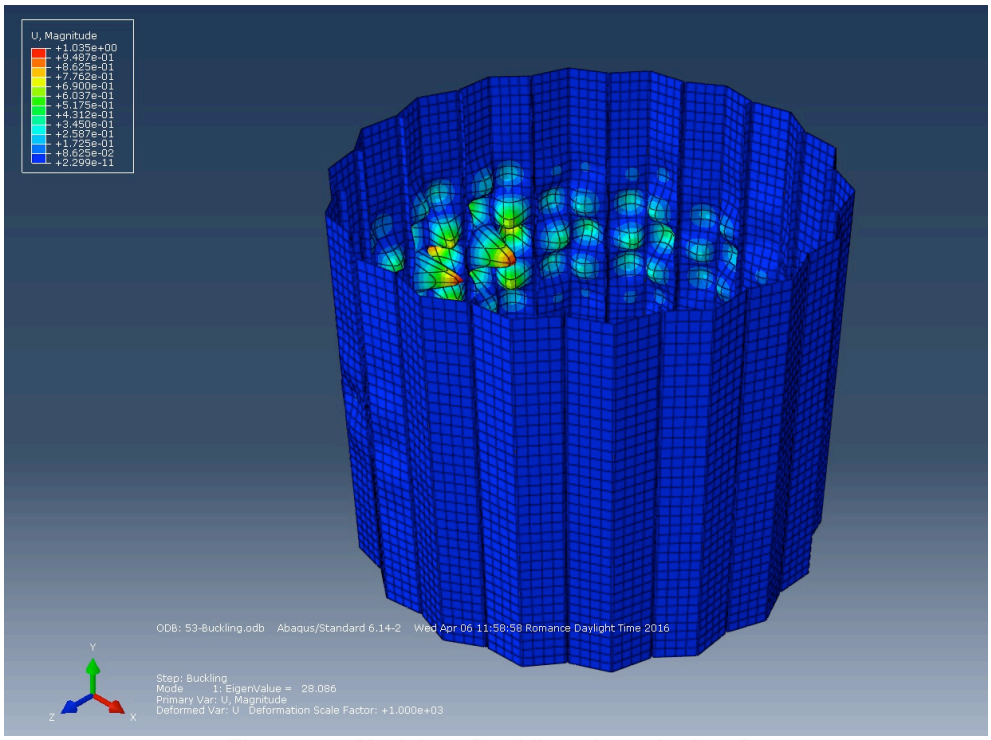

Figure 45 : Model 53, Buckling shape in the 3D.

- **Model 60, length: 8m**

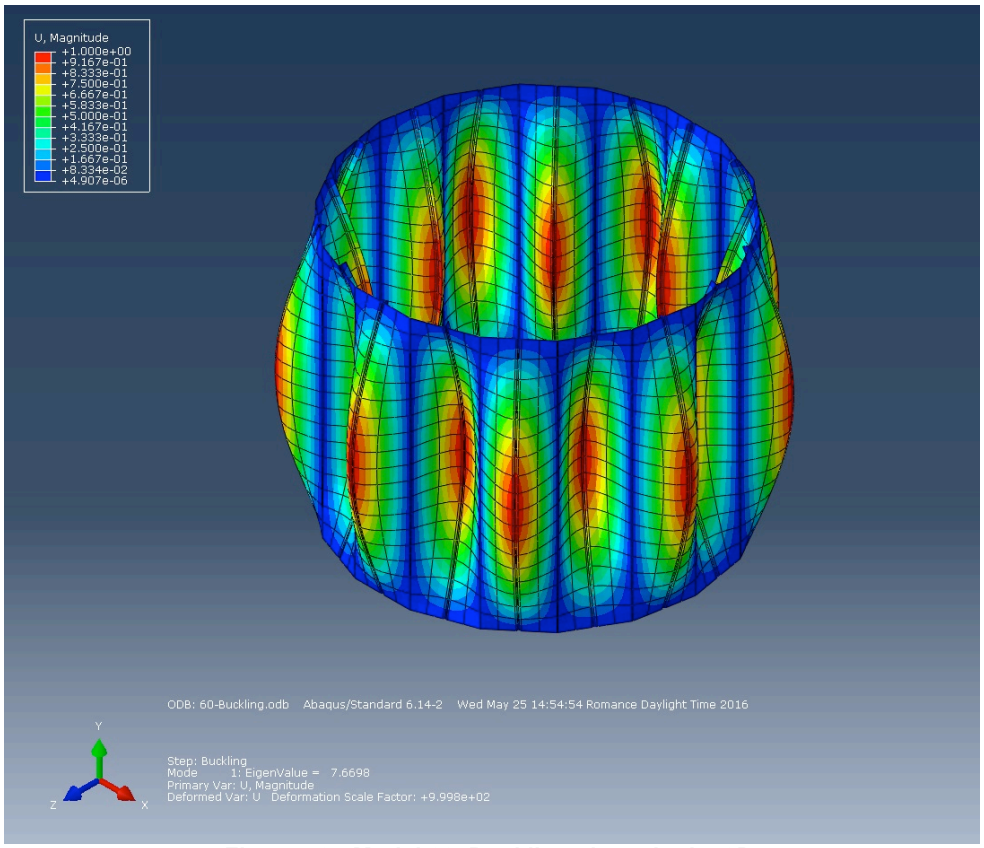

Figure 46 : Model 60, Buckling shape in the 3D.

- **Model 62, length: 8m**

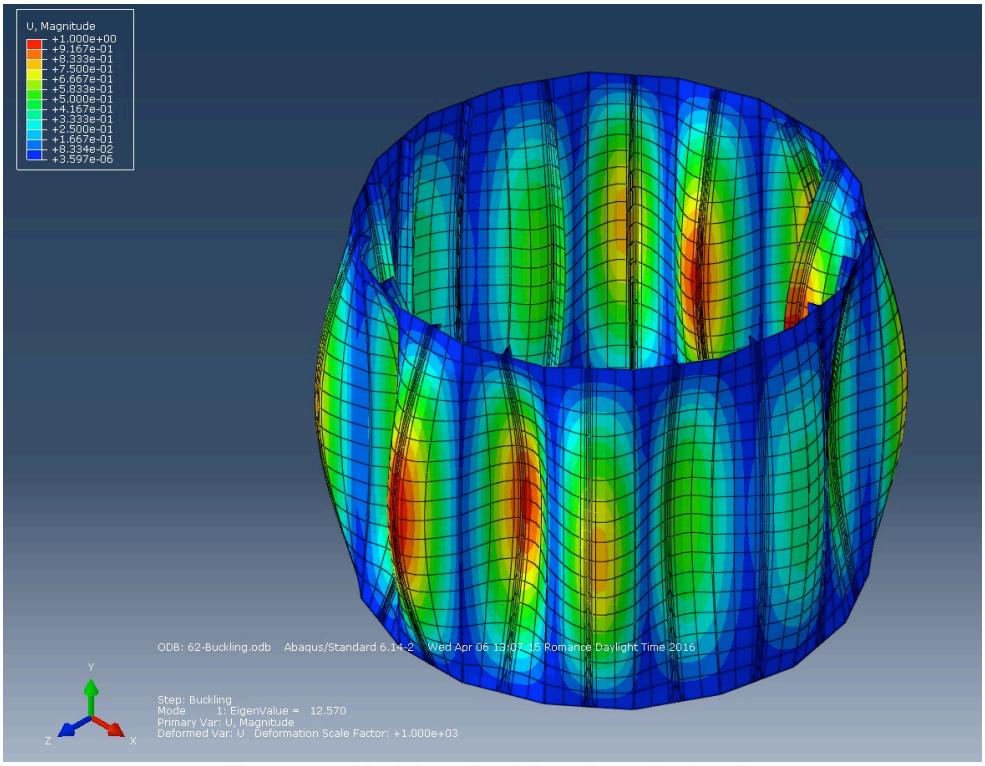

Figure 47 : Model 62, Buckling shape in the 3D.

- **Model 1055, length: 10m**

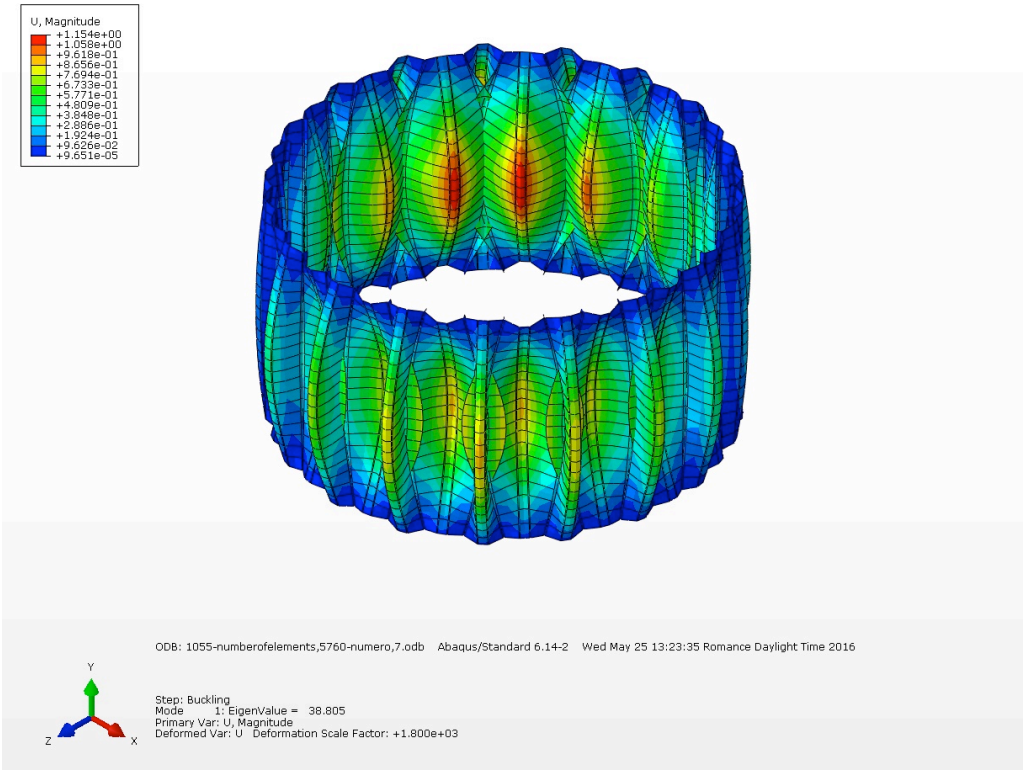

Figure 48 : Model 1055, Buckling shape in the 3D.

- **Model 1055, length: 8m**

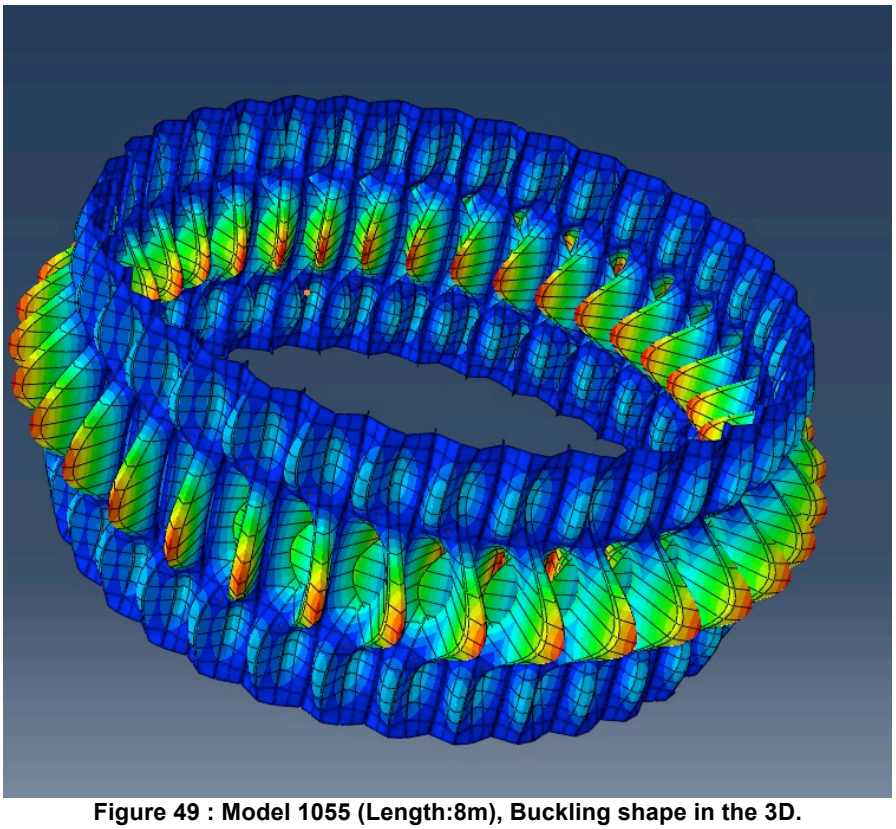

Figure 49 : Model 1055 (Length:8m), Buckling shape in the 3D.

- **Model 1055, length: 6m**

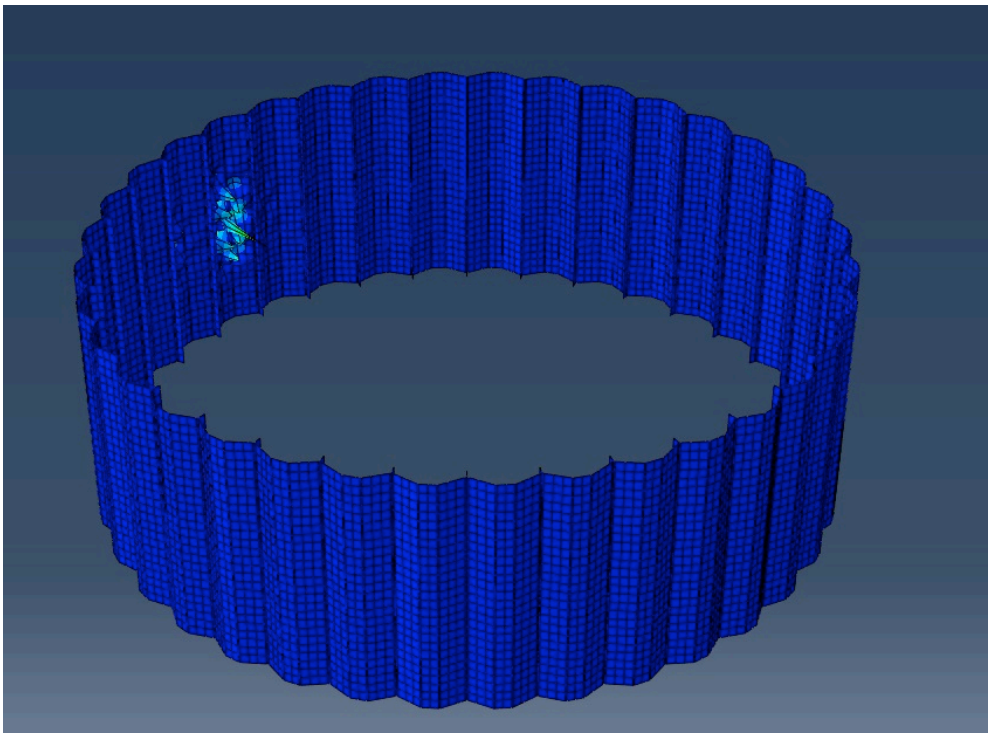

Figure 50 : Model 1055 (Length:6m), Buckling shape in the 3D.

- **Model 55, length: 8m**

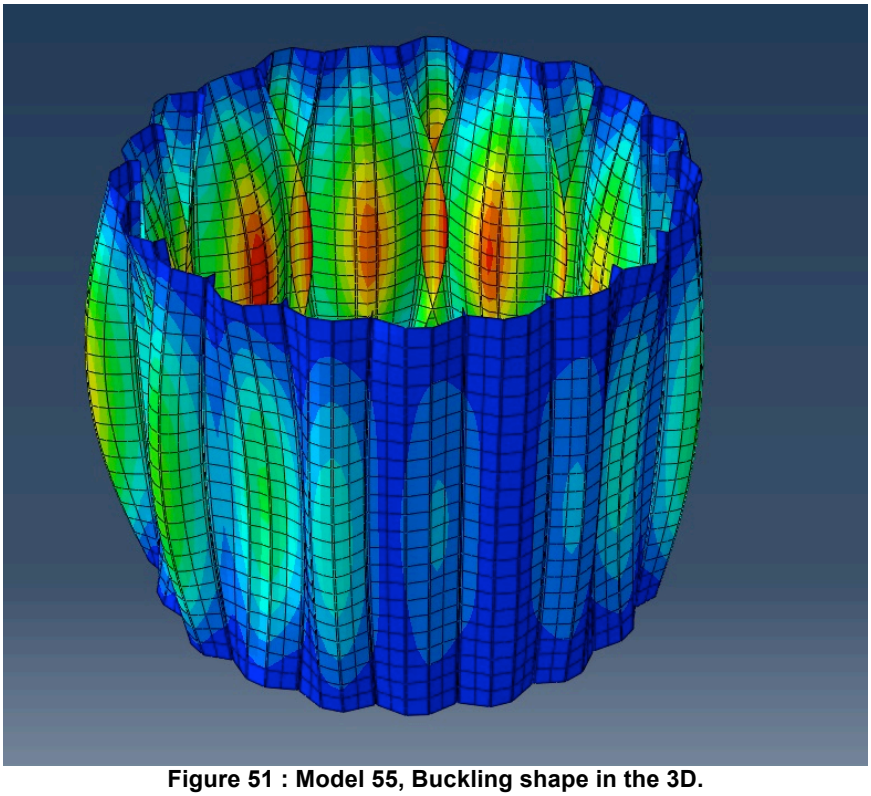

Figure 51 : Model 55, Buckling shape in the 3D.

D. Nonlinear analyses results with several load-displacements curves specified

- **Model 1053**

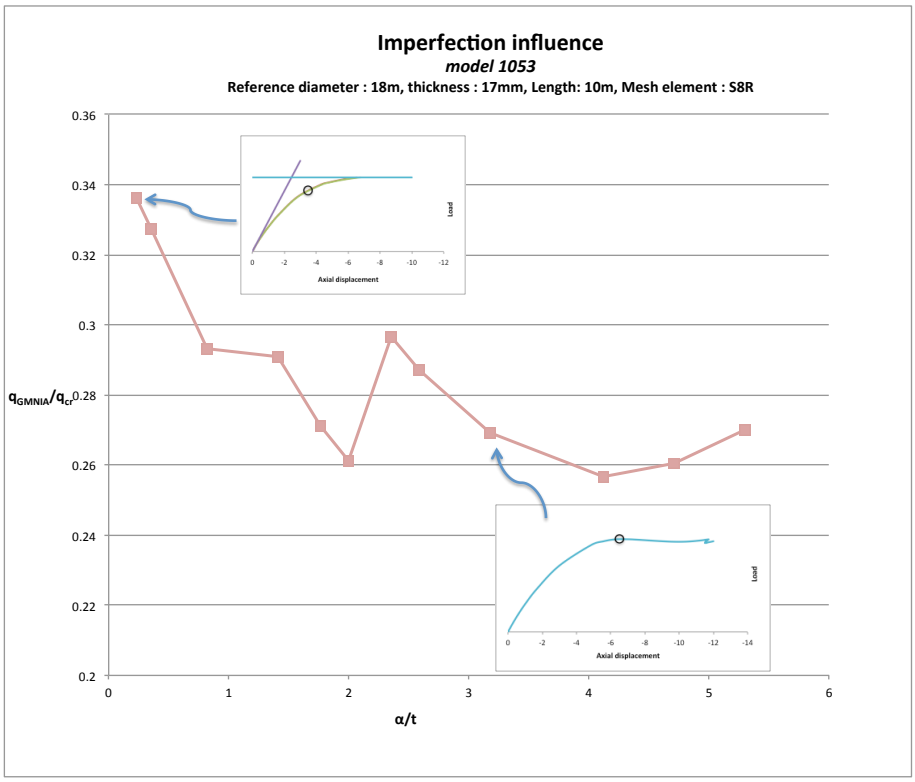

Figure 52 : knockdown factors as a function of the ratio α/t, model 1053 with the load-deflexion curves for specific imperfection sizes.

- **Model 1060**

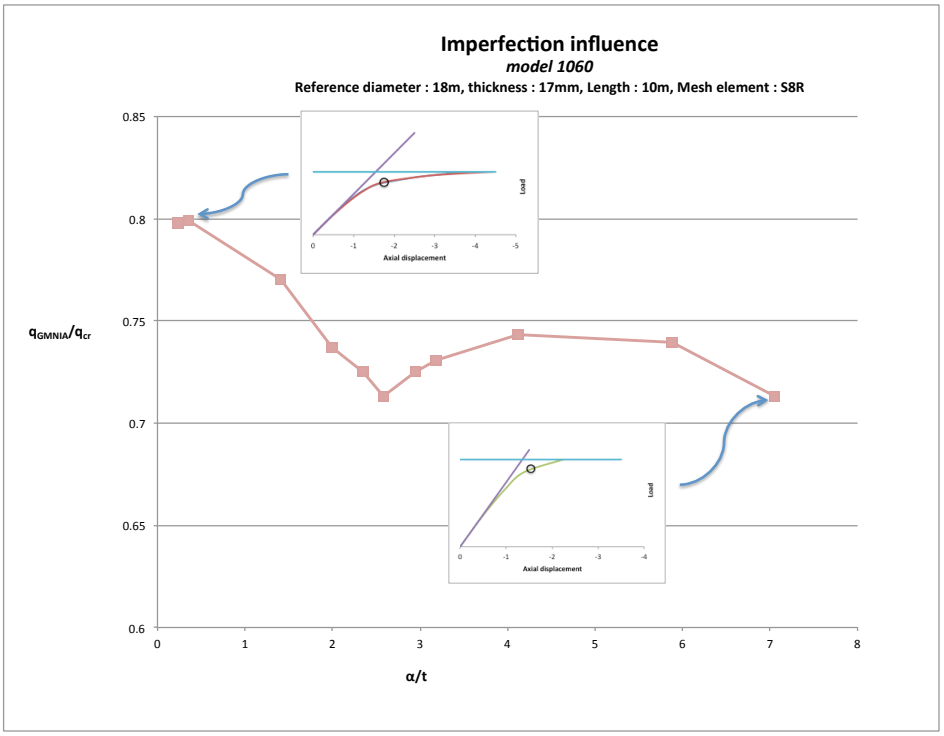

Figure 53 : knockdown factors as a function of the ratio α/t, model 1060 with the load-deflexion curves for specific imperfection sizes.

- **Model 1055**

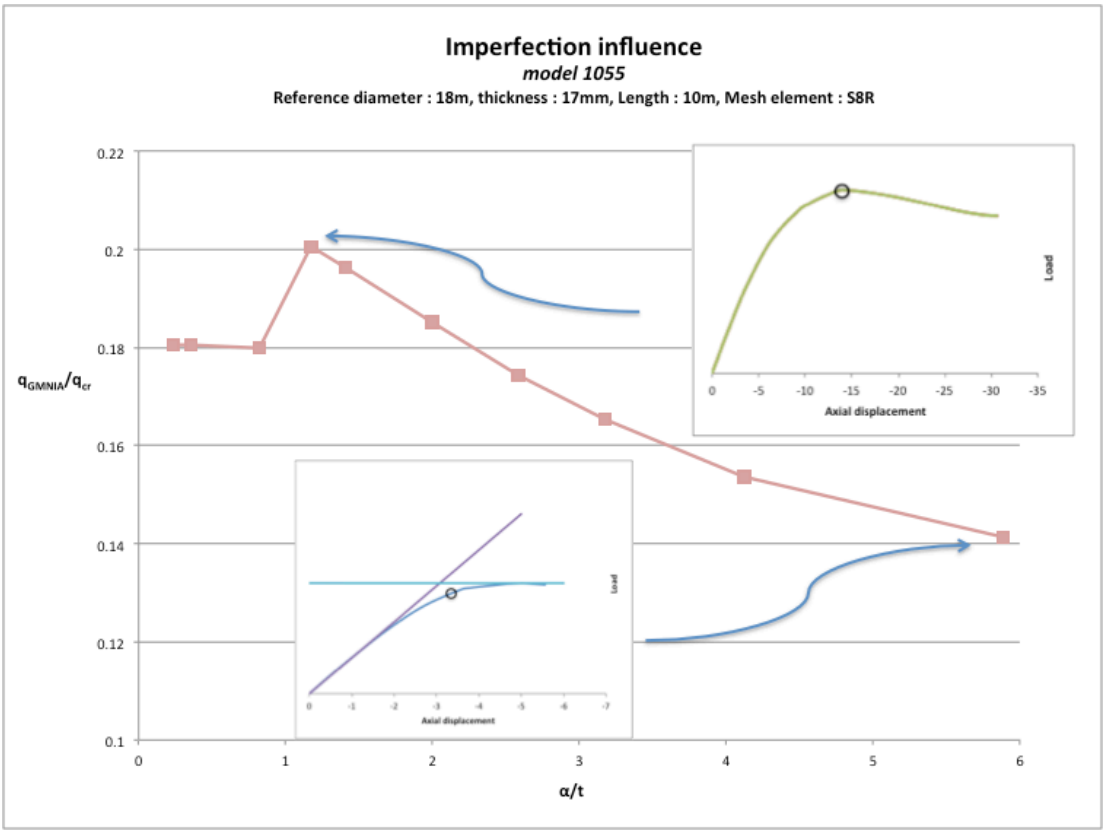

Figure 54 : knockdown factors as a function of the ratio α/t, model 1055 with the load-deflexion curves for specific imperfection sizes.

- **Model 50**

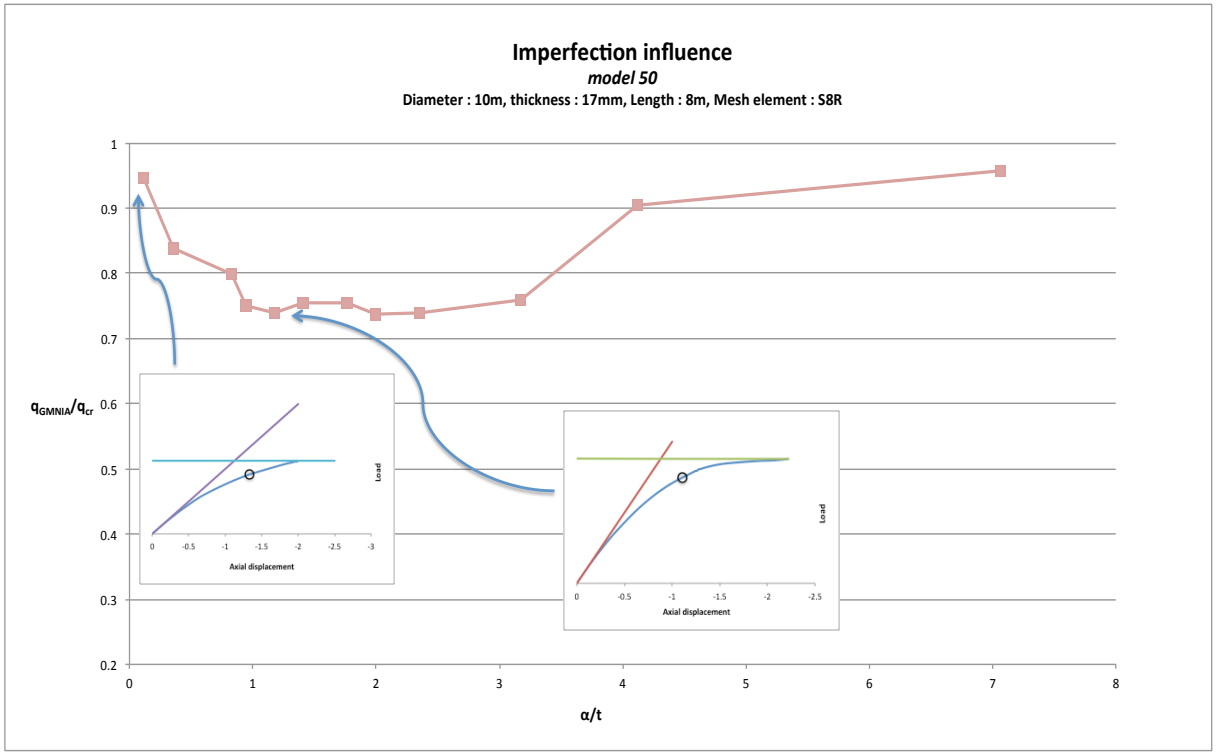

Figure 55 : knockdown factors as a function of the ratio α/t, model 50 with the load-deflexion curves for specific imperfection sizes.

- **Model 51**

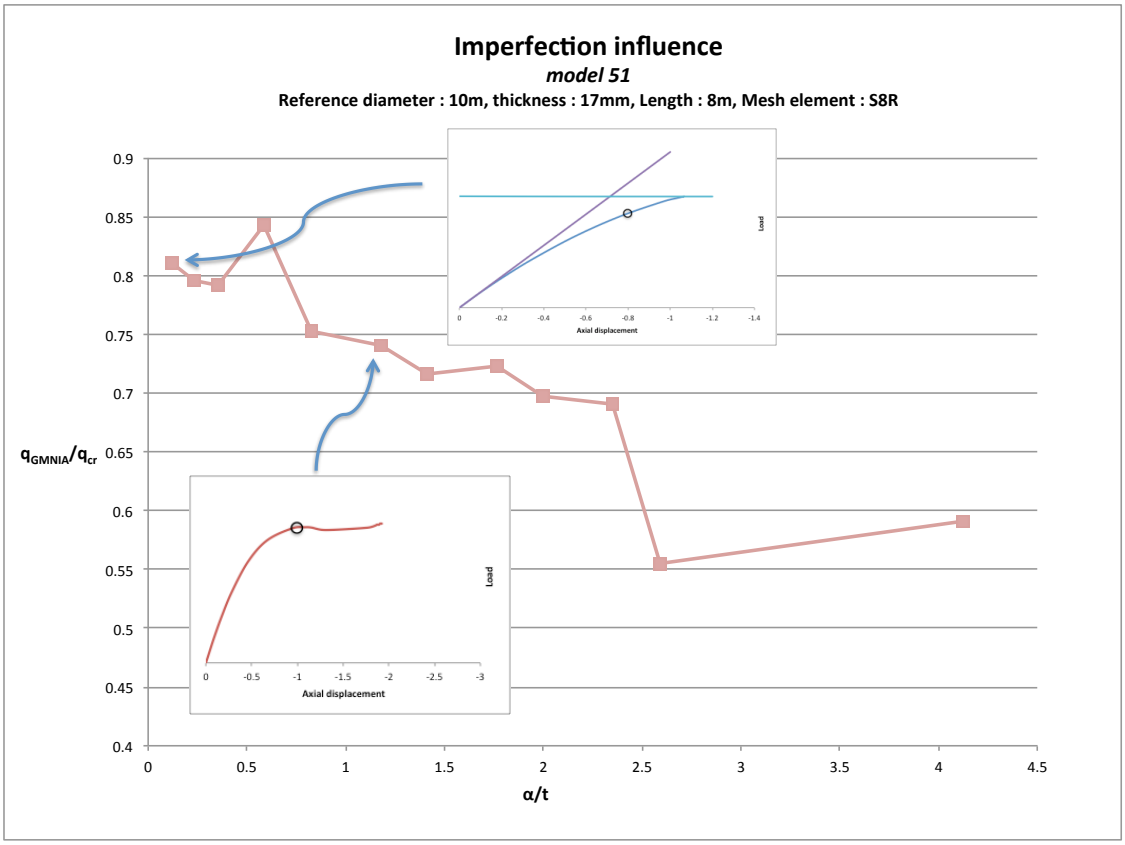

Figure 56 : knockdown factors as a function of the ratio α/t, model 51 with the load-deflexion curves for specific imperfection sizes.

- **Model 52**

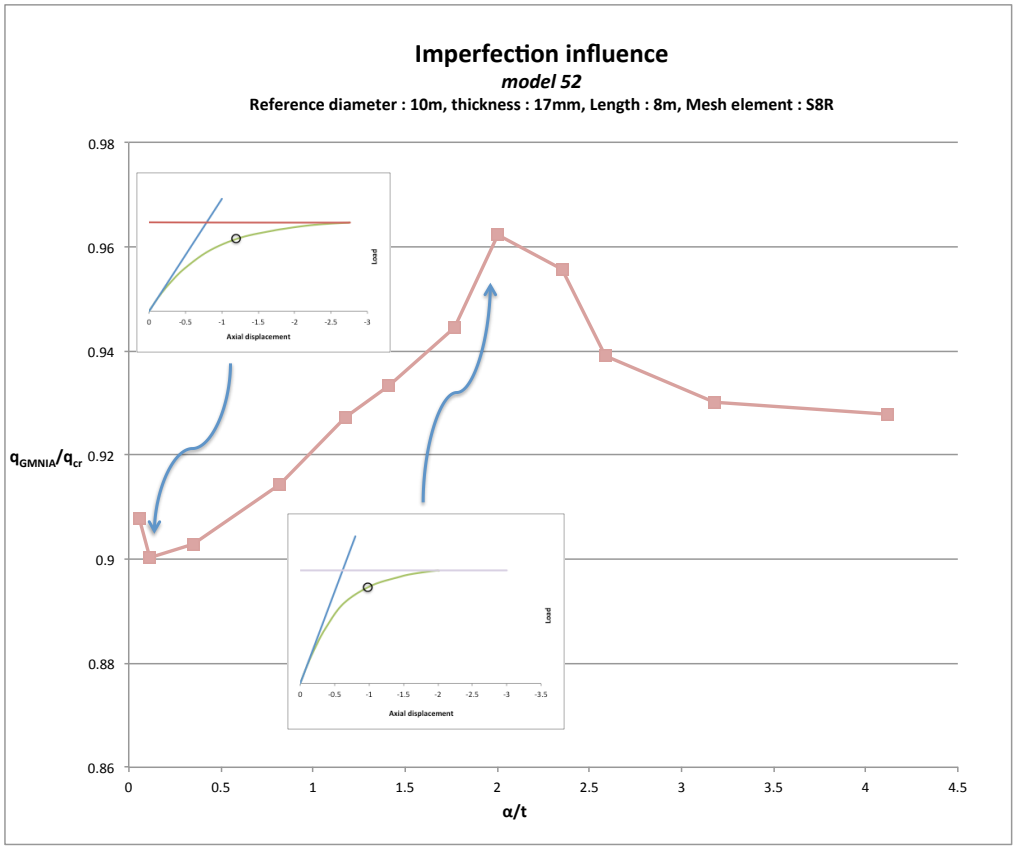

Figure 57 : knockdown factors as a function of the ratio α/t, model 52 with the load-deflexion curves for specific imperfection sizes.

- **Model 53**

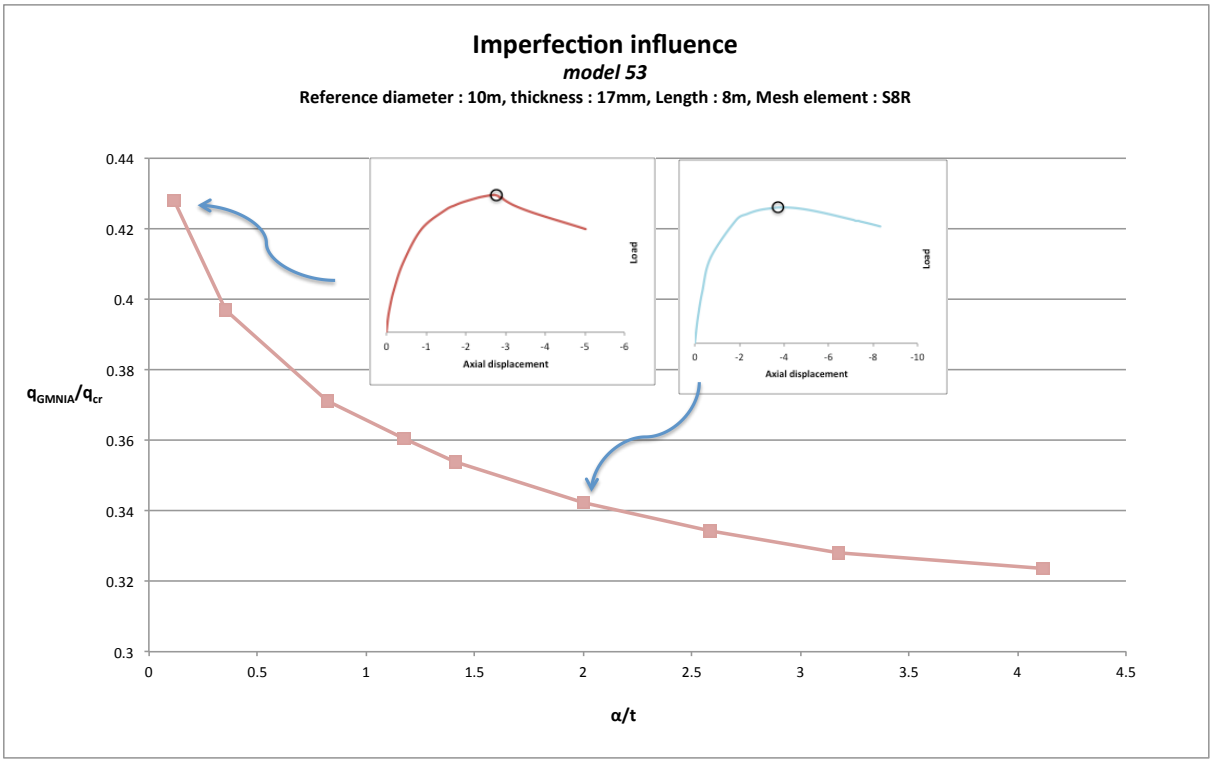

Figure 58 : knockdown factors as a function of the ratio α/t, model 53 with the load-deflexion curves for specific imperfection sizes.

- **Model 60**

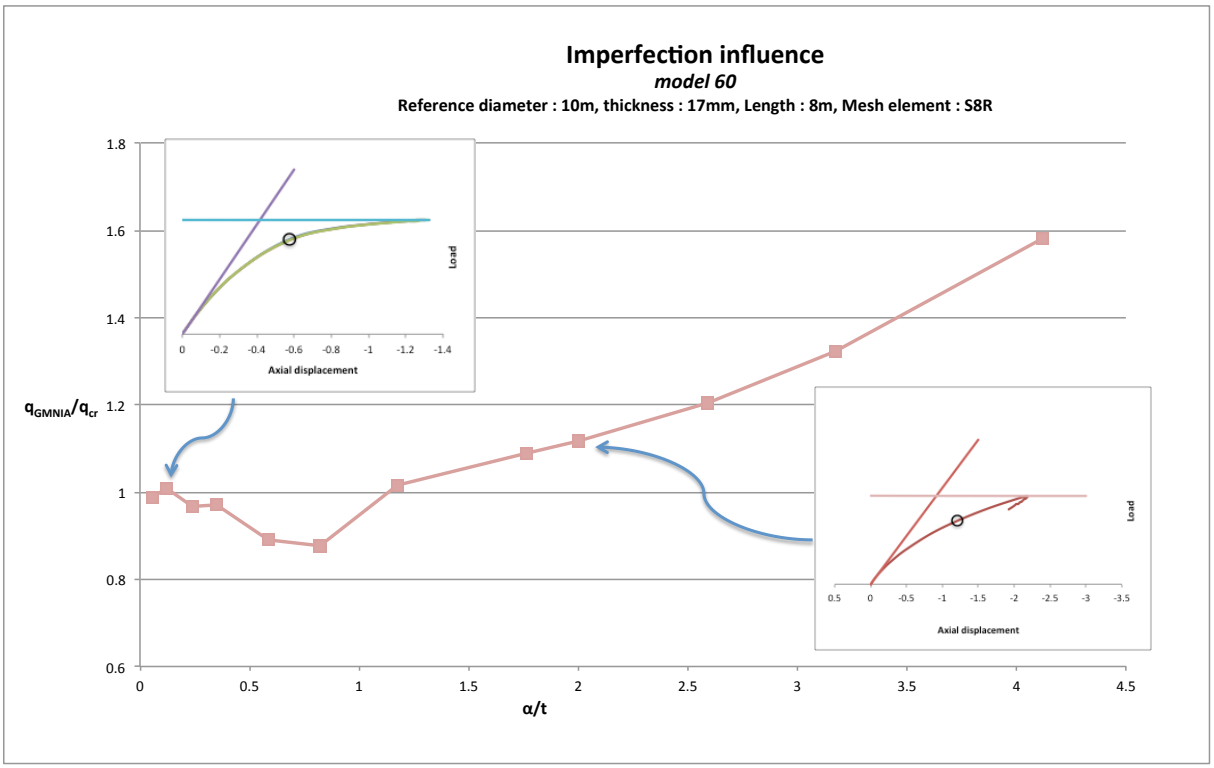

Figure 59 : knockdown factors as a function of the ratio α/t, model 60 with the load-deflexion curves for specific imperfection sizes.

- **Model 62**

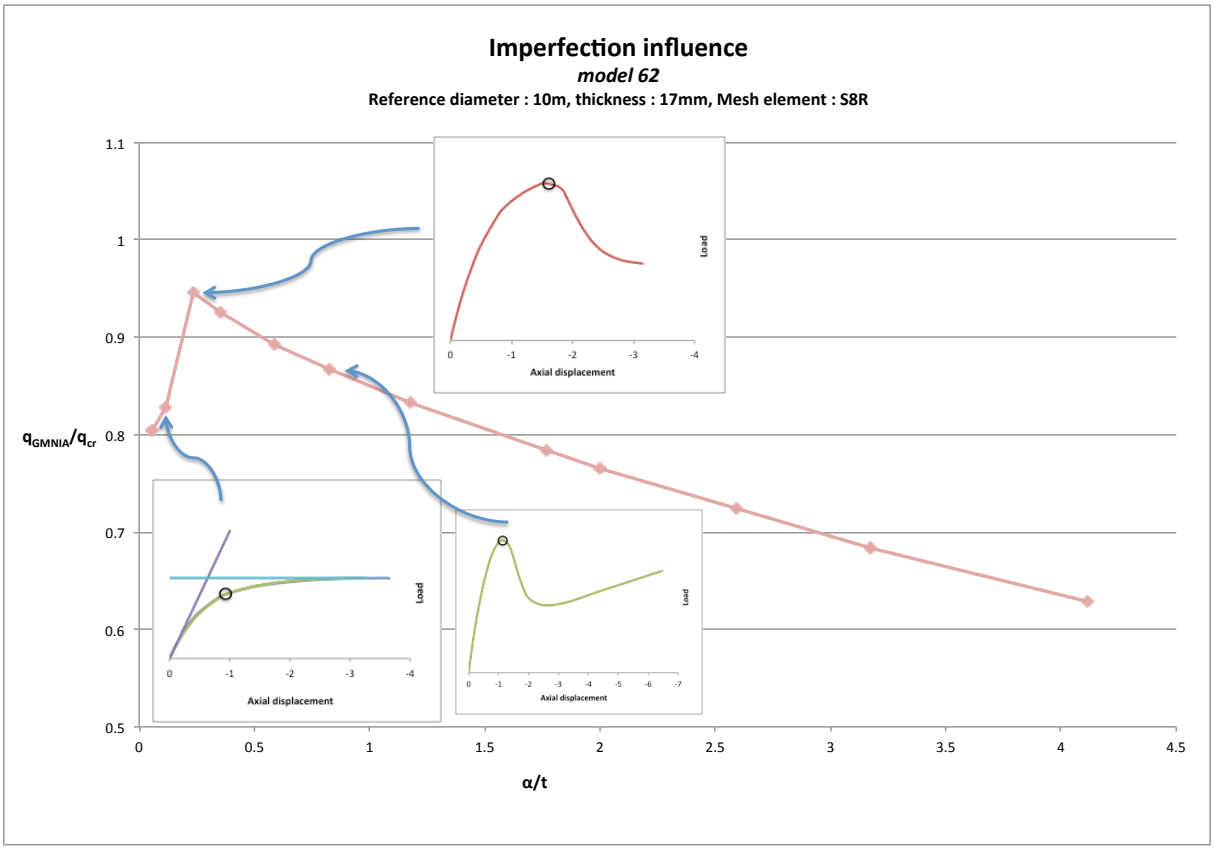

Figure 60 : knockdown factors as a function of the ratio α/t, model 62 with the load-deflexion curves for specific imperfection sizes.

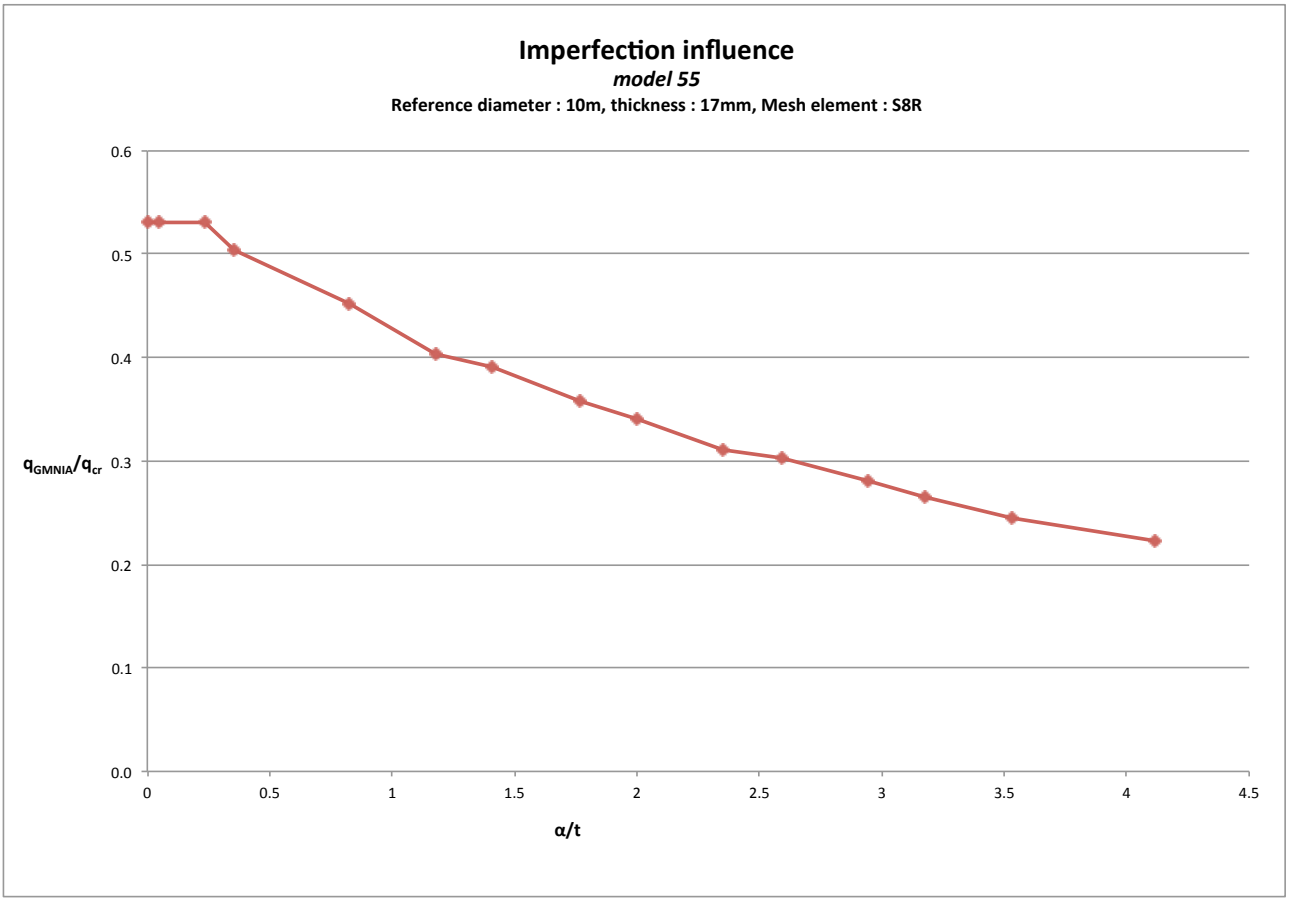

Figure 61 : knockdown factors as a function of the ratio α/t, model 55.

ISSN 1901-7278
DCE Technical Report No. 213